STUDY OF THE STRUCTURAL, ELECTRICAL AND MAGNETIC PROPERTIES OF RARE EARTH YTTRIUM DOPED Mn-Zn FERRITES

M. Phil. Thesis

By

SUBROTO SUBON ACHARJEE

DEPARTMENT OF PHYSICS

KHULNA UNIVERSITY OF ENGINEERING & TECHNOLOGY

KHULNA - 9203, BANGLADESH

JUNE - 2018

STUDY OF THE STRUCTURAL, ELECTRICAL AND MAGNETIC PROPERTIES OF RARE EARTH YTTRIUM DOPED Mn-Zn FERRITES

M. Phil. Thesis

By

SUBROTO SUBON ACHARJEE

ROLL No. 1455502

SESSION: JANUARY - 2014

A THESIS SUBMITED TO THE DEPARTMENT OF PHYSICS, KHULNA UNIVERSITY OF ENGINEERING & TECHNOLOGY, KHULNA - 9203 IN PARTIAL FULFILMENT OF THE REQUIRMENT FOR THE DEGREE OF MASTER OF PHILOSOPHY

DEPARTMENT OF PHYSICS

KHULNA UNIVERSITY OF ENGINEERING & TECHNOLOGY

KHULNA - 9203, BANGLADESH

JUNE - 2018

TO

MY PARENTS

DECLARATION

This is to certify that the thesis work entitled as **"Study of the Structural, Electrical and Magnetic Properties of Rare Earth Yttrium Doped Mn-Zn Ferrites"** has been carried out in partial fulfillment of the requirement for M. Phil. degree in the department of Physics, Khulna University of Engineering & Technology, Khulna - 9203, Bangladesh. The above research work or any part of this work has not been submitted anywhere for the award of any degree or diploma. No other person's work has been used without due acknowledgement.

1. Supervisor

(Prof. Dr. S. S. Sikder)

Candidate

(Subroto Subon Acharjee)

2. Co-Supervisor

(Dr. Mohammed Nazrul Islam Khan)

Acknowledgements

First and foremost, I would like to thank the Almighty for giving me the strength, knowledge, ability and opportunity to undertake this research study and complete it satisfactorily.

I with due respect express my deepest sense of sincere gratitude indebtedness to my supervisor Prof. Dr. Shibendra Shekher Sikder, Department of Physics, Khulna University of Engineering & Technology (KUET), Khulna for his indispensable guidance, erudite discussion, constructive suggestions, fruitful discussion and constant inspiration throughout the research work. He is always ready to provide a lucid explanation of the different concepts involved and critical reading of the script and subsequent corrections are much appreciated. Any mistake that remain is of course mine. Without his constant supervision this thesis work could not be performed.

I am very much indebted to my Co-Supervisor Dr. Mohammad Nazrul Islam Khan, Principal Scientific Officer, Materials Science Division, Atomic Energy Centre, and Dhaka for introducing the present research topic and inspiring guidance and valuable suggestion throughout the research work. It would have not been possible for me to bring out this thesis without his help and constant encouragement.

I am indebted to Professor Dr. Md. Mahbub Alam, Head, Department of Physics; Khulna University of Engineering & technology, Khulna his accurate acceptable direction and instruction was as sweet as honey which was quality with tonic and antibiotic to overcome opposite chronicle.

I am very much grateful to Dr. Sk. Manjura Haque, Head and Chief Scientific Officer, Materials Science Division, Atomic Energy Centre, Dhaka for providing kind opportunity to work in her laboratory for experimental work. Ms. Nazmunnahar Begum, Ms. Jarna Begum and Ms. Arunnahar Irin, Scientific Officer, Materials Science Division, Atomic Energy centre, Dhaka for providing me with technical assistance from time during my research work

I gratefully acknowledge Professor Dr. Md. Abdullah Elias Akhtar and Professor Dr. Jolly Sultana, Department of Physics, Khulna University of Engineering & Technology for his co-operation and inspiration during this work. My thanks are also for Mr. Md. Kamrul Hasan Reza, Associate Professor, Mr.Sujit Kumar Shil,

Mr.Suman Halder, and Mr. Suman Debnath, Assistant Professor, Mr. Probal Roy and Mr. Saifullah, Lecturer, Department of Physics, KUET for their moral supports.

I am very much indebted to Mr. Md. Alamgir Hossain, Assistant Professor, Department of Physics, KUET, and Khulna. I feel and realize that it was not possible to complete my thesis work without his cordial nursery help tendency with generous thinking and expert skillful suggestion and perfect instruction.

I am very much indebted to Prof. Dr. Mohammad Abu Yusuf, Department of Chemistry, Khulna University of Engineering & Technology, and Khulna for his useful suggestion and help to carry out my research work.

I would like to extend my special thanks to Engineer. Md. Ashraful Kabir , Chairman and Engineer S.M. Rezaul Kabir, Principal, BCMC College of Engineering & Technology, Jessore who inspired and helped me highly to reach my goal.

My thanks are also for my Colleagues, Md. Shahidul Alam, Md. Habibur Rahman, Assistant Professor and Md.Abdullah Al Mamun, Lecturer, Department of Social Science & Related Subjects, BCMC College of Engineering & Technology, Jessore. I would also like to thank my well wishers Prodip Kumar Mondal, Kaushik Sarkar, Al-Masud and Md.Deloar Hossain Solid State Physics Lab, KUET.

A very special thank to Mrs. Nandita Saha, spouse of Prof. Dr. S. S. Sikder for her heartfelt encouragement, cares and helps throughout the entire period of M. Phil. program.

My thanks are due to Director, Atomic Energy Centre, and Dhaka for his kind permission to use the Laboratory of Materials Science Division, Atomic Energy Centre, and Dhaka.

My acknowledgement would be incomplete without thanking my parents (Shyama Ranjan Acharjee & Swapan Acharjee), my wife (Protima Chowdhury) and other family members for their multifaceted support and love no matter distance. Words are not enough to express my feelings and sincere thanks to my loving.

I also wish to thank the authority of Khulna University of Engineering & Technology (KUET), for providing me with the necessary permission and financial assistance for conducting this thesis work.

SUBROTO SUBON ACHARJEE

ABSTRACT

Mn-Zn ferrites belong to a group of spinels studied extensively because of their interesting technical properties. The present work focused on rare earth (Y) substituted for Fe in Mn-Zn ferrites are well-known technological magnetic materials used for manufacturing of multilayer chip inductor and applications in various electrical devices. The series of ferrite sample of composition $Mn_{0.5}Zn_{0.5}Y_xFe_{2-x}O_4$ where x = 0.00, 0.02, 0.04, 0.06, 0.08 and 0.10 were prepared by solid state reaction technique sintered at 1200^oC with 2 hours holding time. The X-ray diffraction analysis revealed that rare earth free sample shows formulation of single phase cubic spinel structure with no extra peak but Y substituted for Fe in Mn-Zn samples show additional peaks manifested the formation of secondary phase presumably $YFeO_3$. Lattice constant primarily increase up to x = 0.04 and thereafter decreases. X-ray density of this composition is slightly greater than that of their bulk densities due to existence of some pores in the bulk sample. The average grain size decrease monotonically with increasing Y content while the porosity of studied samples follow the opposite trend. The average grain size has significant influenced on the magnetic properties such as permeability. A significant change in initial permeability has been found to increase or decrease by the amount of Y^{3+} in $Mn_{0.5}Zn_{0.5}Y_xFe_{2-x}O_4$ ferrite. But the initial permeability decreases with increasing Y ions in ferrite except x = 0.06. Relative Quality factor (RQF) signifies the merit of the material from the application point of view and found to have high values for the samples with x= 0.04 and x= 0.08.The saturation magnetization (M_S), coercivity (H_c) and remanent induction (M_r) have been calculated from M – H curve at room temperature. The decrease of M_S with increasing of Y substitutions has been explained as the effect of dilution of Fe^{3+} magnetic moment by nonmagnetic Y^{3+}. The electrical DC resistivity decreases with increasing temperature for all studied samples manifesting semiconducting nature of Y substituted Mn-Zn ferrites. The dielectric constant is found to decrease continuously with increasing frequency and remain almost constant at higher frequency range. Dielectric polarization and conduction process arise due to the local displacements of electrons which in turn gives the dielectric constants.

Contents

CHAPTER-III

EXPERIMENTAL PROCEDURE

CHAPTER-IV
RESULTS AND DISCUSSION

CHAPTER-V
CONCLUSIONS

List of Figures

List of Tables

List of Symbols

Manganese	=	Mn
Zinc	=	Zn
Lanthanum	=	La
Samarium	=	Sm
Gadolinium	=	Gd
Dysprosium	=	Dy
Neodymium	=	Nd
Yttrium	=	Y
Europium	=	Eu
Nickel	=	Ni
Cobalt	=	Co
Magnesium	=	Mg
Iron	=	Fe
Cerium	=	Ce
Terbium	=	Tb
Bohr mgneton	=	μ_B
Bragg's angle	=	θ
Bulk density	=	d_B
Charge of electron	=	e
Capacitance	=	C
Coercivity	=	H_C
Cross-sectional area of toroids	=	S
Curie temperature	=	T_C
DC resistivity	=	ρ_{dc}
Dielectric constant	=	ϵ'
Diffraction angle	=	θ
Chemical bath deposition	=	CBD
Exchange integral	=	J
Exchange coupling constant	=	J_{ij}
Exchange correlation length	=	L_0

Face centered cubic	=	fcc
Frequency	=	f_r
Rare Earth	=	RE
Imaginary part of initial permeability	=	μ"
Impedance	=	Z
Inductance	=	L
Initial permeability	=	μ_i
Inter planner spacing	=	d
Loss factor	=	tanδ
Magnetization	=	M
Magnetic field	=	H
Transmission electron microscopy	=	TEM
Scanning electron microscopy	=	SEM
Vibrating sample magnetometer	=	VSM
Electromagnetic interference device	=	EMI
Nelson-Riley function	=	F(θ)
Number of turns	=	N
Boltzmann constant	=	K_B
Permeability of in free space	=	μ_0
Relative quality factor	=	RQF
Absolute temperature	=	T
Real part of initial permeability	=	μ'
Activation Energy	=	Ea
Remanent Induction	=	M_r
Resistance	=	R
Resistivity	=	ρ
Saturation magnetization	=	M_S
Saturation induction	=	M_r
Oersted	=	Oe
Yttrium aluminum garnet	=	YAG
Yttrium iron garnet	=	YIG
Susceptibility	=	χ
X-ray density	=	d_X
X-ray diffraction	=	XRD
Wavelength	=	λ

INTRODUCTION

1.1 Introduction

Ferrites pervade almost every sphere of modern technology. The present day technology owes a lot to the ferrite industry ranging from the very ordinary radio sets to the complicated and exhaustive hardwires involved in computers, ferrites have found their way to prove their importance. As a result, at high frequency applications eddy current losses are negligible in ferrites indispensible materials in telecommunications and in the electronic industry where frequencies in the range of 10^3 to 10^{11}Hz have to handle. Ferrites are ferromagnetic materials composed of certain double oxide of Fe and another metal which have two unequal sublattices and are ordered antiparallel to each other. Spinel ferrites are playing important role in ferromagnetic materials due to their incredible magnetic properties particularly in the radio frequency region due to physical flexibility, high electrical resistivity, mechanical hardness and chemical stability.

Mn–Zn ferrites belong to the group of soft ferrite materials characterized by high magnetic permeability low power loss, high saturation magnetization and relatively high curie temperature, have widely served as fundamental materials in electronic and information industries, being used as recording heads, choke coils and communication pulse transformers, antenna roads, loading coils, deflection yokes, magnetic amplifiers, electromagnetic interference device (EMI), power transformers, splitters and so on. Moreover, Mn-Zn ferrites are very important in biomedicine as magnetic carries fir bioseperation, enzymes and proteins immobilization.

The Mn-Zn ferrites preferred over other ferrites for their high initial permeability, low losses, high saturation magnetization and relatively high Curie temperature. The very well known fact that substituted SiO_2, CaO, Ta_2O_5, Nb_2O_5 in to Mn-Zn ferrites have excellent magnetic properties at high frequency [1.1-1.2]. It is well established that in Mn-Zn ferrites are simple cubic structure most of the Zn^{2+} ions occupy in tetrahedral A-sites [1.3] which results in a lowering of Fe^{3+} in octahedral A-sites. Higher values of electrical resistivity could be achieved by incorporating the divalent cations as well as by controlling their others properties. The grain growth of introducing divalent cations in to the Mn-Zn ferrites produces grain boundaries which may act as barrier for electrons flow, causing the declination of eddy current losses.

The surface morphology, magnetic and transport properties depend on the microstructure, particle size, surface to volume ratio [1.4], milling technique, preparation temperature concentration of the dopants and impurities of the new prepared materials. Hence it is possible to incorporate metallic ions to the ferrite Mn-Zn to enlargement their electronic and magnetic properties significantly [1.5]. The structural, magnetic and electrical properties are found to be sensitive to their composition and microstructure. There are many chemical processing techniques are available to prepare of ferrites. The choice of an appropriate synthetic procedure often depends on the desired properties and the final applications. Among these methods the solid state reaction technique has several advantages over others for the preparation of the specimen.

The influence of different rare earth atoms like La, Sm, Gd, Nd, Dy, Ce, Th, Y, Eu on the properties of ferrites. Rare earth (RE) ions can be divided into two categories: one with the radius larger than Fe-ions [1.6]. The rare earth ions commonly reside at the octahedral sites by replacing Fe^{3+} ions and have been limited solubility in the spinel lattice due their large ionic radii [1.7]. Ferrimagnetisms in ferrite is largely governed by Fe-Fe interaction means the spin coupling of the 3d electrons. Rare earth ions enter the spinel lattice, the RE-Fe interactions also appears 4f-3d coupling, which is to changes in the magnetization and Curie temperature. Rare earth doped materials can occupy different positions on the octahedral and tetrahedral sites and alter the microstructure, magnetic, transport as well as optical properties. The RE ion forms the orthoferrite phase. The occupation of RE ions on B-sites impedes the motion of Fe^{2+} in the conduction process in ferrite, thus causing an increase in resistivity. Some considerations must be taken into account to incorporate rare earth ions into the Mn-Zn ferrites due to the large dimension of RE ions. Introducing a very poor amount of rare earth ions may significantly changes the microstructure, electrical, magnetic as well as optical properties of the ferrites composites. By introducing optimally rare earth materials in to the ferrite specimen like Mn-Zn ferrites it is possible to develop good magnetic materials. Rare earth Gd^{3+} and Eu^{3+} ions replace the metallic cations in tetrahedral A-sites or octahedral B-sites to improve various properties of the samples [1.8 - 1.11].

Mn-Zn ferrites have a great importance from the technological view points. Researcher continues their efforts to find out optimum parameters of ferrites, like high saturation magnetization, high permeability, high resistivity etc. However, till now, as

far as the effect of Fe replacement by Yttrium (Y) ions on the properties of Mn-Zn ferrites concerned systematic study. For this reason, in this work we report some systematic investigation on composition, temperature and frequency dependent magnetic, dielectric and electrical properties of Mn-Zn ferrites with the addition of Y.

1.2 The Aims and Objectives of the Resent Work

This main objective has been the search for the best suited composition and preparation parameters for optimum performance of ferrite samples in respect of frequency response permeability and dielectrics. Ferrites are especially convenient for high frequency uses because of their high resistivity. The high frequency response of the complex permeability is therefore very in determining the convenient frequency range in which a particular ferrite material can be used. The mechanism of eddy current losses and damping of domain wall motion can be understood from the relative magnitudes of the real and imaginary part of the complex permeability.

The rare earth substituted different ferrites are becoming the promising materials applications. Addition of small amount of rare earth ions to Mn-Zn ferrites samples produces a change in their magnetic and electrical as well as structural properties depending upon and amount of rare elements like Y used. The main purpose of this work is to amalgamate Mn-Zn ferrites of composition $Mn_{0.5}Zn_{0.5}Y_xFe_{2-x}O_4$ where [x = 0.00, 0.02, 0.04, 0.06, 0.08 and 0.10] and, hence to study the effect of substitution of rare earth Yttrium ions (Y^{3+}) doped on the surface morphology, saturation magnetization, the loss of quality factors, the electrical resistivity of Mn-Zn ferrites.

The main objectives of the present research are as follows:

- Preparation of various $Mn_{0.5}Zn_{0.5}Y_xFe_{2-x}O_4$ (where x = 0.00, 0.02, 0.04, 0.06,0.08, 0.10) samples by solid state reaction technique.
- Determination of crystal structure (X-ray diffraction), density and porosity of the samples.
- Investigation of surface morphology, microstructure and compositional analyses using Scanning Electron Microscopy (SEM).
- Study of complex initial permeability as a function of frequency (100Hz-120MHz) using Wayne Kerr Impedance Analyzer.

- Investigation of specific magnetization process using Vibrating Sample Magnetometer (VSM).
- Measurement of complex dielectric constant of various compositions over a range of frequency (20Hz-120MHz)
- Measurement of resistivity using Electrometer Cathley.

Finally, it is expected to use powder particles as starting materials may give uniform microstructure exhibiting better magnetic and electrical transport properties. With the substitution of rare earth metals in the Mn-Zn ferrite system permeability and magnetic properties are expected to be improved. Thus this system will have further good technological application in high frequency range. In our research in soft magnetic materials and in rare earth metal doped ferrites, Bangladesh may develop a profitable electronic industry

1.3 Experimental Reason for This Research Work

$Mn_{0.5}Zn_{0.5}Y_xFe_{2-x}O_4$ samples has been prepared by standard solid state reaction technique. High purity powders of MnO (99.9%), ZnO (99.9%), Y_2O_3 (99.9%), Fe_2O_3 (99.9%) will be mixed thoroughly in an appropriate amount mixing will be performed in both dry and acetone. The mixed powders will be calcined at high temperature. After calcinations toroid and disk shaped sample will be prepared and will be sintered at temperatures. The experimental methods that have been used in this work are as follows:

- The prepared sample would be characterized in terms of their crystal structure, unit cell parameters and phase presents in the prepared sample with the help of X-ray diffractometer (XRD) in the material science division, Atomic Energy Center (AEC), Dhaka
- Sintering of the samples has been carried out in a microprocessor controlled high temperature furnace department of Physics, Khulna University of Engineering & Technology(KUET) , Khulna
- Surface morphology of the samples has been investigated using scanning electron microscope in the material science division, AEC, Dhaka.

- Permeability, magnetic loss factor and quality factor as function of frequency have been determining using impedance analyzer in the department of Physics, KUET, Khulna
- Magnetizations of the samples have been measured as a function of field using vibrating sample magnetometer (VSM) in the material science division, AEC, Dhaka
- AC electrical resistivity as a function temperature has been studied with the help of electrometer in the department of Physics, KUET, Khulna
- Dielectric properties as a function of frequency have been studied with the help of inductance meter department of Physics, KUET, Khulna

Finally the structural properties of Fe replaced Y in Mn-Zn ferrites such as grain size, lattice parameters is modified due to the incorporation Y^{3+} ions. The saturation magnetization, the quality factor, electrical resistivity of Mn-Zn ferrites are also expected to improve and accumulated results has been interpreted on the basis of existing theories of magnetic.

1.4 Application of Ferrites

Ferrites are primarily used as inductive components in a large variety of electronic circuits such as low noise amplifiers, filters, voltage controlled oscillators, impedance matching networks for instance. The basic components to produce the inductance are very soft ferrite and a metallic coil. Multilayer chip inductors for high frequency circuit's applications use sheets made of dielectric ceramics instead of ferrite industry. Rare earth ferrites are used widely now-a-days due to their following applications:

- Biomedical (e.g., hip and joint replacements)
- Ball bearings and hard face seals
- Oil drilling
- Automotive and marine engines
- Industrial machines
- Magneto-optical materials
- Magnetic refrigerant materials

- Neutron absorber material for atomic reactor and catalysts for chemical reactions
- Microwave technology, manufacture of fluorescent powder for color TV sets etc.

1.5 Review of the Earlier Research Work

Remarkable properties such as high permeability, high quality factor, high stability of initial permeability with temperature and time, high resistivity, controlled coercive force etc. have appositely placed Mn-Zn ferrites as high demandable materials to both researchers and manufacturers. Hilpert [1.12] first focused of the usefulness of ferrites at high frequency applications. Ferrites were developed into commercially useful materials by Snoek [1.13] and his associates at Philips research laboratories in Holland during years 1933 – 1945. The greatest advances for the Mn-Zn ferrites were made in the mid-sixties fast centuries. Mn-Zn ferrites with composition $Mn_{0.3}Zn_{0.4}Fe_{2.3}O_4$ have high permeability because of low value of magnetostriction and anisotropy [1.14]. As soft magnetic materials Mn-Zn ferrites have been proved to be the smart candidate of highest rank. The requisites for modern ferrite are so many in numbers that only extensive research in this field can meet the huge demand of technology.

Takai [1.15] in Japan at the same time was engaged in the research on the ferrite materials. He was particularly looking for high permeability materials of cubic structure. He found suitable materials in the form of mixed spinel of the type (Me-Zn).Fe_2O_4, where Me represents metal Like Mn, Ni, Mg, Cu, etc. Many Scientists and technologists have focused their attention on the improvement of electromagnetic properties of the ferrite by divalent ions substitution. Generally, the divalent metal ions (Me^{2+}); Ni, Zn, Cu, Mg, Mn, Co or mixtures of these are substituted in different spinel ferrites. Spinel ferrites are extremely important for academic and technological applications. The physical properties such as structural, electrical and magnetic properties are governed by the type of magnetic ion residing on the tetrahedral A –site and octahedral B-site of the spinel lattice and the relative strength of the inter and inter-sub lattice interaction. Divalent ion substitutes have different sitting preferences for the two sites (‘A’ and ‘B’) in the spinel structure and can change many properties as an effect of modified cation distribution in the ferrite. On the basis of site distribution of Me^{2+} ions and the strength of the exchange interaction among magnetic

ions, the influent influence of Me^{2+} substitution on electromagnetic properties can be explained.

Sharma *et. al* [1.16] manganese ferrite ($MnFe_2O_4$) nanoparticles were synthesized using chemical bath deposition (CBD) method and characterized by XRD and TEM to determine different properties of nanoparticles. The results obtained showed the formation of manganese ferrite nanoparticles with an average particle size are in good agreement with previous reported experimental results and displayed good magnetic properties. Magnetic properties were determined using VSM. Due to simplicity and low cost of this process, it could be used for synthesis of ferrites nanoparticles. These materials may be used in drug delivery systems, electronic devices and water remediation.

Isfahani *et. al* [1.17] have been studied the magnetic properties of nanostructured $Mn_{0.5}Zn_{0.5}Fe_2O_4$ ferrites. He has reported reduced saturation magnetization can be attributed to the prevailing effect of spin canting. The M – T curve of nanoscale ferrite gives evidence that the mechanic-synthesized material exhibits higher Neel temperature than bulk sample. The enhanced Neel temperature can be attributed to the effect of strengthening of the A-O-B super-exchange interaction in the mechno-syntheized spinel phase.

Ping Hu *et. al* [1.18] have been investigated the effect of heat treatment temperature on crystalline phases formation, microstructure ant magnetic properties of Mn-Zn ferrite by XRD, DTA, SEM and VSM. Ferrites decomposed Fe_2O_4 and Mn_2O_3 after annealing at 550^oC in air, which have poor magnetic properties. With continuously increased annealing temperature, Fe_2O_4 and Mn_2O_3 impurities were dissolved when the annealing temperature rose above 1100^oC. The sample annealed at 1200^oC showed pure Mn-Zn ferrite phase, which fine crystalline, uniform particle size and large saturation magnetization and lower coercivity.

Ahmed *et. al.* [1.19] reported the effect of rare earth ions on the structural, magnetic and electrical properties of $(Mn_{0.5}\ Zn_{0.5})RE_{0.05}\ Fe_{1.95}O_4$ ferrites where RE = Tb, La, Ce, and Th. Rare earth ions formed orthoferrite ($REFeO_3$) phase and formation of these secondary phase in ferrite during sintering process was governed by the type and the amount of RE^{3+} in used. It was found that the molar magnetic susceptibility for rare earth substituted samples were smaller than pure ferrite. T_c and electrical resistivity increased with increasing rare earth ions in Mn-Zn ferrites.

Zhao *et. al* [1.20] reported influence of Gd on magnetic properties of $Ni_{0.7}Mn_{0.3}Gd_xFe_{2-x}O_4$ ferrites. It has been found the crystallite sizes decreased when Gd ions were doped into Ni-Mn ferrites. With Gd substitution, when x > 0.06 all Gd ions could not enter into the ferrite lattice but resided at grain boundary. The maximum content of Gd^{3+} ions in ferrite lattices was substituted when x = 0.06. Razlescu *et. al* [1.21] investigated the influence of RE like Yb, Er, Dy, Tb, Gd, Sm substitution on structure, magnetic and electrical properties of $Li_{0.3}Zn_{0.4}Fe_{1.96}RE_{0.04}O_4$ ferrites. They found that RE_2O_3 facilitated the formation of secondary phases at grain boundary which suppressed the grain growth. The results also showed that the Curie point shifted to lower temperature and increased the electrical resistivity.

Sun *et. al* [1.22] reported the effect of Fe substitution by La and Gd on the structure, magnetic and dielectric properties of $Ni_{0.5}Zn_{0.5}Fe_{2-x}RE_xO_4$ ferrites. It was found that the relative density of sintered bodies decreased and the lattice parameter increased with increasing RE ion substitution. La and Gd both tend to increase the cut-off frequency, decrease the initial permeability and magnetic loss tangent which could be explained by a combination of low density, small grain size, secondary phase formation and more lattice defects. The low loss tangent values resulted mainly from the reduction in eddy current loss due to the higher electrical resistivity with increasing RE ion.

Nakamura [1.23] reported on frequency dispersion of permeability in ferrite composite materials. The permeability increases with increasing density of composite materials. As the ferrite content decreases both the real and imaginary parts of the low frequency permeability is significantly reduced, and the peak frequency of imaginary part of permeability shifts toward higher frequency.

Zhong *et. al*. [1.24] the effects of RE_2O_3 (RE = Sm, Gd, Ce and Y) doping on the microstructure and magnetic properties of Mn-Zn ferrite have been investigated. The single spinel phase structure can be maintained with the doping amounts up to 0.07 *wt.*%. A refined grain structure and uniform grain size distribution can be obtained in the optimally doped materials. With a small amount of doping, the permeability increases significantly and the magnetic loss and coercivity decrease, but further increase of the doping content leads to a reduced permeability and increased loss and coercivity. To achieve excellent magnetic properties, the optimized doping amount for Sm_2O_3 or Gd_2O_3 is 0.01 *wt.* %, while for Ce_2O_3 or Y_2O_3 is 0.03 *wt.* %. The

sample with 0.01 *wt*. % Sm_2O_3 shows the magnetic properties with permeability, loss, and coercivity of 2586, 316W/ kg, and 24A/m, respectively, at 200 mT and 100 kHz.

In the present work, the attempt is made to systematically investigate the structural, magnetic, electric and dielectric properties of rare earth (RE = Y^{3+}, x = 0.00, 0.02, 0.04, 0.06, 0.08 and 0.10) substituted $Mn_{0.50}Zn_{0.50}RE_xFe_{2-x}O_4$ spinel ferrites and it is prepared by Standard Ceramic Method. This composition can be used for technological applications

1.6 Outline of the Thesis

The thesis has been configured into five chapters which are as follows:

Chapter 1: Introduction

In this chapter, presents a brief introduction to Mn-Zn ferrites and organization of thesis. This chapter incorporates background information to assist in understanding the aims and objectives of this investigation, and also reviews recent reports by other investigators with which these results can compared.

Chapter II: Theoretical Background

In this chapter, a briefly describe theories necessary to understand magnetic materials as well as ferrites, classification of ferrites, cation distribution, super exchange interaction, two sub lattices modules etc. have been discussed in details.

Chapter III: Experimental Background

In this chapter, the experiment procedures are briefly explained along with description of the sample preparation, raw materials. This chapter deals with mainly the design and construction of experimental and preparation of ferrite samples. The fundamentals and working principles of measurement set up are discussed.

Chapter IV: Results and Discussion

In this chapter, results and discussion are thoroughly explained. The various experimental and theoretical studies namely Effect of Rare Earth Metal Substitution on the Structural, Electrical and Magnetic properties of Mn-Zn Ferrites are presented and discussed step by step.

Chapter V: Conclusion

In this chapter, the results obtained in this study are summarized. Suggestions for future works on these studies are included.

Finally a complete list of references and publications as been given towards the end of this chapter.

THEROETICAL BACKGROUND

2.1 Rare Earth Ferrites

In 1948, L. Neel announced his celebrated theoretical contribution on ferrimagnetism. This deal with the basic phenomenon of "spin-spin interaction" takes place in the magnetic sublattices in ferrites. The stage was now set for development of microwave ferrite devices. In 1956, Neel, Bertaut, Ferrat and Pauthenet discovered the garnet ferrite class of materials. This type of ferrite material has three sublattices and also referred to as rare earth iron garnets. These materials, through having a magnetization lower than spinel ferrite, possess extremely low ferromagnetic line width. The rare earth substituted different ferrites are becoming the promising materials for different applications. Addition of small amount of rare earth ions to ferrite samples producing a change in their magnetic and electrical as well as structural properties depending upon the types and the amount of rare earth elements used. The rare earth elements are all metals, and the group is often referred to as the "rare earth metals." These metals have many similar properties and that often causes them to be found together in geologic deposits. They are also referred to as "rare earth oxides" because many of them are typically sold as oxide compounds. Rare earth elements are not as "rare" as their name implies. Thulium and lutetium are the two least abundant rare earth elements - but they each have an average crustal abundance that is nearly 200 times greater than the crustal abundance of gold [2.1].

The rare earth ions have unpaired 4f electrons and the strong spin orbit coupling of the angular momentum. Moreover, 4f shell of rare earth ions is shielded by $5s^2 5p^6$ and almost not affected by the potential field of surrounding ions. Doping rare earth ions into spinel type ferrites, the occurrence of 4f-3d couplings which determine the magneto-crystalline anisotropy in spinel ferrite can also improve the electric and magnetic properties of spinel ferrites [2.2-2.5]. Spinel ferrites ceramic are widely used in microwave devices to control transmission path, frequency, amplitude and phase of microwave signals. Accurate dielectric and magnetic properties measurement at the operational frequency and temperature ranges are needed for optimized development of these devices, as well as to assist in the manufacture of the ferrite [2.6]. The structured magnetic materials have an interesting area of study because of its possible applications in a variety of widely areas ranging from information technology to biotechnology [2.7]. The properties of ferrites are being

improved due to the increasing trends in ferrite technology. It is believed that there is a bright future for ferrite technology. Ferric magnetism in ferrite is largely governed by Fe-Fe interaction, i.e. the spin coupling of the 3d electron. In view of the great interest of rare earth doped Mn-Zn ferrites, both their technological applications and theoretical understanding of the mechanisms involved, the present work is aimed at finding the effect Y ions. A large number of workers are engaged in research to bring about improvement on the qualities of rare earth doped Mn-Zn ferrites.

2.2 Types Ferrites

In terms of the magnetic properties, ferrites are often classified as soft and hard which refers to their low or high coercivity respectively. Exhibiting dielectric properties means that even through electromagnetic waves can pass through ferrites, they do not readily conduct electricity. This also gives them an advantage over irons, nickel and other transition metals that have magnetic properties in many applications because these metals conduct electricity. Ferrites are classified into two categories based on their coercive field strength.

They are:

(i) Soft ferrite with coercive field strength < 10 Oe

(ii) Hard ferrite with coercive field strength > 125Oe

In terms of the crystal structure, ferrites are often classified crystal structure, ferrites are of following types. [2.12]

- Cubic ferrites
- Spinel Ferrite
- Hexagonal ferrites
- Garnet
- Ortho- ferrite

The present research work is a spinel ferrites, therefore it has been discussed in detail the spinel ferrites only.

2.2.1 Cubic Ferrites

General formula of cubic ferrites is $MO.Fe_2O_3$, where M is divalent metal ion like Mn, Ni, Fe, Co, Zn, Mg, Cd, Cu, etc. Cobalt ferrite like $CoO.Fe_2O_3$ is magnetically hard, but all other cubic ferrites are magnetically soft. Usually, ferrites have spinel structures, often called ferro-spinel because their crystal structure is closely related to that of mineral spinel $MgO.Al_2O_3$. In case of ferrites the divalent

ions replace Mg and trivalent ions replace Al. In all cases the ionic radii of the substitution ion should be between about 0.5 to 1A^{o}.

2.2.2 Spinel Ferrites

Soft ferrites entirely belong to spinel family. They are also called cubic ferrite. Spinel is the most widely used family of ferrite. High values of electrical resistivity and low eddy current losses make them ideal for their use at microwave frequencies. The spinel structure of ferrite as possessed by mineral spinel $MgA_{l2}O_4$ was first determined by Bragg and Nishikawa in 1915 [2.8 - 2.9]. The chemical composition of a spinel ferrite can be written in general as MFe_2O_4 where M is a divalent metal ion such as Co^{2+}, Zn^{2+}, Fe^{2+}, Mg^{2+}, Ni^{2+}, Cd^{2+}, Cu^{2+} or a combination of these ions. Spinel is an important class of mixed metal oxides, which has the general chemical composition of $A^{2+}B^{3+}O_4^{2-}$. Normally A is a divalent metal such as Mg, Mn, Fe, Zn, Cu etc and B is trivalent metal such as Ti, Fe, Al and Co. The structure consists of a cubic closed-packed array of 32 oxide ions, which forms 64 tetrahedral holes and 32 octahedral in a unit cell. There are two main types of spinels:

(i) In normal spinel all the A^{2+} cations occupy one of the available tetrahedral holes and all the B^{3+} cations occupy other of the octahedral holes. Normal spinels represented as $A^{3+}[B_2^{3+}]O_4^{2-}$ [2.10].

(ii) In inverse spinels all the A^{2+} cations and half of the B^{3+} cations are in octahedral and other half of the B^{2+} cations are in the tetrahedral holes. Inverse spinels are represented as $B^{3+}[A^{2+}B^{3+}]O_4^{2-}$.

The magnetic properties of spinel ferrites are generally influenced by composition and cation distributions. Variation of cation distribution between the cationic sites lead to different electrical and magnetic properties even if the composition of cations over A and B sites is determined by their ionic radius, electronic configuration and electrostatic energy in the spinel lattice

2.2.3 Hexagonal Ferrites

Hexagonal ferrites widely used in microwave applications, have an axis of symmetry, C and high magnetocrystalline anisotropy. This was first identified by Went, Rathenau, Gorter and Van Oostershout 1952 [2.11] and Jonker, Wijn and

Braun 1956. The preparation of hexagonal ferrites is the ceramic technique is almost same as that of spinels. During the pressing the grains are oriented by a magnetic field in order to align the C-axis of all crystallites in the same direction. As a result, sample similar to a perpendicular to magnetization direction, a gyro-resonance effect is observed. There are two types of hexagonal ferrites:

(i) M-type ferrites are derived from Ba or Sr-ferrites, whose formulae are $BaFe_{12}O_9$ and $SrFe_{12}O_9$, by partial substitution of Al^{3+} ions for Fe^{2+} ions which causes the magnetization and magneto crystalline anisotropy field to increase; by substitution of the groups $Ti^{4+}M^{2+}$ or $Ge^{4+}M^{2+}$ (with M^{2+} = Co, Ni, Zn, Mg, etc) for Fe^{3+} ions, which causes both the magnetization and the anisotropy field to decrease.

(ii) W-type are derived from Ba-ferrites whose formula is $Ni_2BaFe_{16}O_{27}$, by partial substitution of Al^{3+} ions for Fe^{3+} ions, causing an increment in magnetization and anisotropy field; by partial substitution of Co^{2+} for Ni^{2+} causes anisotropy field to decrease keeping magnetization unchanged. These ferrites are used in circulators with resonance frequencies lower than those M-type.

2.2.4 Garnets

Garnets refer to a group of mixed oxides with chemical formula $A_3^{3+}B_5^{3+}O_{12}^{2-}$, where A^{3+} is a rare earth or Yttrium ions. The B^{3+} ions form two anti-parallel sub-lattices composed of 16 octahedral and 24 tetrahedral sites. The A^{3+} ions form a third sublattice of 24 dodecahedral sites in which each A^{3+} is surrounded by 8 oxygen ions located at the corners of a polyhedron with12 faces and 18 edges. 24 A^{3+} ions enter into dodecahedral sites. Examples of garnets are Yttrium Iron Garnet (YIG) and Yttrium Aluminum Garnet (YAG) etc., YIG with chemical composition $Y_3^{3+}Fe_5^{3+}O_{12}^{2-}$, has a spontaneous magnetization that arises from unequal number of Fe^{3+} ions in each of two sub-lattices.

The mineral garnet refers to group of mixed oxides, of which the widely known on has the chemical formula $Mn_3A_{l2}Si_{13}O_{12}$, or equivalently $3MnO.A_{l2}O_3.3Si_2O_3$ single magnetic garnets have the general formula.

$$3M_2O_3.\ 5\ Fe_2O_3 = 2\ M_3^{3+}Fe_5^{3+}O_{12}$$

It is to be noted that in magnetic garnets the 24 positive charge units per formula units are divided unequally between the ferrites ions (15 units) and another

species of trivalent ions (9 units). Technically metal garnets are those with M = Sm, Eu, Gd, Tb, Dy, Ho, Er, Tm, Yb and Yttrium. They are known as rare garnets. A code system has been adopted to name them. REG stands for the rare –earth garnets, GDIG for gadolinium-iron garnet (Gd_3 Fe_5O_{12}) etc. Garnets crystallize in the cubic system with two fifths of the ferrite ions forming a bcc lattice, like ferrospinel, the garnets too. Patch a large number (160) of ions in eight unit's formula unit cell. The lattice constant is nearly 12.5^{o}A about 50% larger than those ferrospinel.

2.2.5 Ortho-ferrites

Ortho-ferrites have the general formula $MFeO_3$, where, M is a large trivalent metal ion, such as rare-earth ion or Y. They crystallize in a distorted pervoskite structure with an orthorhombic unit cell. These ortho-ferrites show a weak ferromagnetism, which has been attributed to the small canting in the alignment of two anti-ferromagnetically coupled lattices. The canting angle is of the order of 10^{-2} radian but is sufficient to introduce a small net ferromagnetic moment perpendicular to the antiferromagnetic axis.

2.3 Soft Magnetic Materials

The wide variety of magnetic materials can be divided into two groups, the magnetically soft and the magnetically hard. Soft magnetic materials are those materials that are easily magnetized and demagnetized. They have low magneto crystalline anisotropy resulting in reduced coercivity and high permeability. They typically have intrinsic coercively less than 1000 Am^{-1}. They are used primarily to enhance and/or channel the flux produced by an electric current. The important parameter, often used as a figure of merit for soft magnetic materials, is the high relative permeability ($\text{where } \mu_r = \frac{B}{\mu_0 H}$), which is a measure of how readily the material responds to the applied magnetic field. The other main parameters of interest are the coactivity, the saturation magnetization and the electrical conductivity.

The types of applications for soft magnetic materials fall into two main categories: AC and DC. In DC applications the material is magnetized in order to perform an operation and then demagnetized at the conclusion of the operation, e.g. an electromagnet on a crane at a scrap yard will be switched on to attract the scrap steel and then switched off to drop the steel. In AC applications the material will be continuously cycled from being magnetized in one direction to the other, throughout

the period of operation, e.g. a power supply transformer. A high permeability will be desirable for each type of application but the significance of the other properties varies.

For DC applications the main consideration for material selection is most likely to be the permeability. This would be the case, for example, in shielding applications where the flux must be channeled through the material. Where the material is used to generate a magnetic field or to create a force then the saturation magnetization may also be significant. For AC applications the important consideration is how much energy is lost in the system as the material is cycled around its hysteresis loop. The energy loss can originate from three different sources: (1) hysteresis loss, which is related to the area contained within the hysteresis loop; (2) eddy current loss, which is related to the generation of electric currents in the magnetic material and the associated resistive losses and (3) anomalous loss, which is related to the movement of domain walls within the material. Hysteresis losses can be reduced by the reduction of the intrinsic coercivity, with a consequent reduction in the area contained within the hysteresis loop.

2.3.1 Soft Ferrites

Soft ferrites are those that can be easily magnetized or demagnetized. This shows that soft magnetic materials have low coercive field and high magnetization that is required in many applications. At high frequency metallic soft magnetic materials simply cannot be used due to the eddy current losses. Therefore, soft ferrites, which are ceramic insulators, become the most desirable material. These materials are ferrimagnetic with a cubic crystal structure and the general composition $MO.Fe_2O_3$, where M is a transition metal such as nickel, manganese, magnesium or zinc. The magnetically soft ferrites first came into commercial production in 1948. The hysteresis loop for a soft ferrite should be thin and long, therefore the energy loss is very low in soft magnetic material. Example are Ni, Fe, Co, Mn etc. They are used in transformer cores, inductors, recording heads and microwave devices [2.12]. Soft ferrites have certain advantages over other electromagnetic materials including high resistivity and low eddy current losses over wide frequency ranges.

Mn-Zn ferrite, sold commercially as ferroxcube, can be used at frequencies up to 10MHz, for example in telephone signal transmitters and receivers and in switch mode power supplies (also referred to as AC-DC converters). For these type of

application the driving force to increase frequency is to allow miniaturization. Additionally, part of the family of soft ferrites, are the microwave ferrites, e.g. yttrium iron garnet. These ferrites are used in the frequency range from 100MHz to 500GHz, for waveguides for electromagnetic radiation and in microwave devices such as phase shifters.

2.3.2 Hard Ferrites

Hard ferrites are difficult to magnetize or demagnetize. Hard magnets are characterized by high remnant inductions and high coercivities. They generally exhibit large hysteresis losses. Hard ferrite referred to as permanent magnets retain their magnetism after being magnetized. Hard ferrite likes Ba-ferrite, Sr-ferrite, Pb-ferrite are used in communication device operating with high frequency currents because of their high resistivity, negligible eddy currents and lower loss of energy due to Joule heating and hysteresis. These are found useful in many applications including fractional horse-power motors, automobiles, audio- and video- recorders, earphones, computer peripherals, and clocks. The magnets can also be used to moderate demagnetizing fields and hence can be used for applications such as permanent magnet motors. The hexagonal ferrite structure is found in both $BaO.6Fe_2O_3$ and $SrO.6Fe_2O_3$, but Sr ferrites have superior magnetic properties.

2.4 Magnetic Exchange Interaction

In physics, the exchange interaction is a quantum mechanical effect without classical analogue which increases or decreases the expectation value of the energy or distance between two or more identical particles when their wave functions overlap. For example, the exchange interaction results in identical particles with specially symmetric wave function (bosons) appearing closer together than would be expected distinguishable particles, and identical particles with spatially anti symmetric wave functions (fermions) appearing further apart. The exchange interaction is the mechanism responsible for ferromagnetism, among other consequences.

The electron spin of the two atoms Si and Sj which is proportional to their product .The exchange energy can be written as universally in terms of Heisenberg Hamiltonian [2.13]

$$H = -\Sigma J_{ij}\, S_i.S_j = -\Sigma J_{ij}\, S_i\, S_j \cos\phi \quad , \qquad (2.1)$$

Where Jij is the exchange integral represents the strength of the coupling between the spin angular momentum i and j and φ is the angle between the spins. It is well known that the favored situation is the one with the lowest energy and it turns out that there are two ways in which the wave functions can combine there are two possibilities for lowering the energy by H.

These are:

a. If Jij is positive and the parallel spin configuration ($\cos\phi = 1$) the energy is minimum.
b. If Jij is negative and the spins are ant parallel ($\cos\phi = -1$) energy is maximum. This situation leads to ant ferromagnetism.

2.5 Super Exchange Interaction

The magnetic interaction in magnetic oxide ferrites cannot be explained on the basis of direct interaction because of the following facts:

(i) The magnetic ions are located too far apart from each other shielded by the non magnetic anion i.e., oxygen. This is because these are not band type semiconductor [2.14] .The non magnetic anion such as oxygen is situated in the line joining magnetic cations.

(ii) Super exchange interaction appears, i.e. indirect exchange via anion p-orbital that may be strong enough to order the magnetic moments.

This p-orbital of an anion (center) interact with the d orbital of the transitional metal cations.

Three major types of super exchange interactions in spinel ferrites are: J_{AB}, J_{BB}, and $J_{AA.}$ Ferromagnetic oxides are one kind of magnetic system in which there exist at least two in equivalent sub lattice for the magnetic ions. The anti parallel alignment between these sub lattices (ferrimagneting ordering) may occur provided the inter sub lattice (J_{AB}) exchange interaction are ant ferromagnetic and some requirements concerning the signs and strength of the intra-sub lattice (J_{AA}, J_{BB}) exchange interactions are fulfilled.

Since usually in ferromagnetic oxides the magnetic cations are surrounded by bigger oxygen anions (almost excluding the direct overlap between cation orbital) magnetic interactions occur via indirect super exchange interactions depends both on the electronic structure of the cations and their geometrical arrangement [2.15]. In

most of ferromagnetic oxides the crystallographic and electronic structure give rise to ant ferromagnetic inter and intra-sub lattice competing interactions.

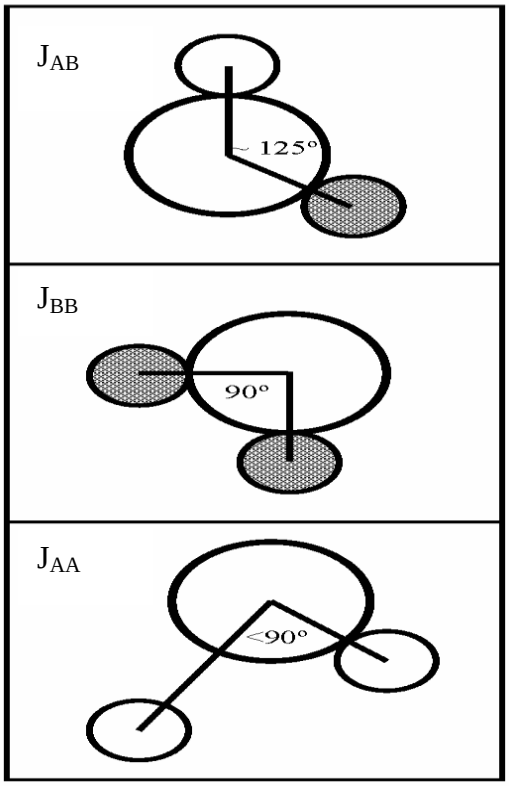

Figure 2.1: Three major types of super exchange interactions in spinel ferrites are as follows: J_{AB}, J_{BB} and J_{AA}. The small empty circle is A-site, the small solid circle is B-site, and the large empty circle is oxygen anion.

The magnitude of negative exchange energies between the two magnetic ions M and M' depend upon the distances from these ions to the oxygen ion O^{2-} via which the super exchange takes place and on the angle M-O-M'(ϕ). According to the super exchange theory the angle ϕ= 180° gives rise to the greatest exchange energy, and this energy decrease very rapidly as the distance between the ions increases. The magnetic properties of the spinel ferrites are governed by the type of magnetic ions residing on the A and B-sites and the relative strengths of the inter-sub lattice (J_{AB}) and intra-sub lattice (J_{AA}, J_{BB}) exchange interactions.

2.6 Theory of Initial Permeability

Initial permeability describes the relative permeability of a material at low values of B. The maximum value for μ in a material is frequently a facing of between 2 and 5 or more above its initial value. Low flux has the advantage that every ferrite

can be measured at that density without risk of saturation. This consistency means that comparison between different ferrite is easy.

For high frequency application, the desirable property of a ferrite is the high initial permeability with low loss. The present goal of the most of the recent ferrite researches is to fulfill this requirement. The initial permeability μ_i is defined as the derivative of induction B with respect to the initial field H in the demagnetization state.

$$\mu_i = \left|\frac{dB}{dH}\right|_{H \to 0,\, B \to 0} \tag{2.2}$$

At microwave frequency and also in low anisotropic materials, dH and dB may be in different directions. The permeability is thus a tensor character. In the case of amorphous materials containing a large number of randomly oriented magnetic atoms the permeability will be scalar. As we have

$$B = \mu_0 (H+M) \tag{2.3}$$

and susceptibility

$$\chi = \frac{dM}{dH} = \frac{d}{dxH}\left(\frac{B}{\mu_0} - 1\right) = \frac{1}{\mu_0}(\mu - 1) \tag{2.4}$$

The magnetic energy density

$$E = \frac{1}{\mu_0} \int H.dB \tag{2.5}$$

For time harmonic fields $H = H_0$ Sin wt. The dissipation can be described by a phase difference between B^+ and B.

Permeability is namely defines as the proportional constant between the magnetic field induction B and applied intensity H:

$$B = \mu H \tag{2.6}$$

If a magnetic material is subjected to an AC magnetic field as given below:

$$H = H_0 e^{i\omega t} \tag{2.7}$$

Then it is observed that the magnetic flux density B experiences a delay. The delay is caused due to presence of various losses and is thus expressed as

$$B = B_0 e^{i(\omega t - \delta)} \tag{2.8}$$

Where δ is the phase angle and marks the delay of B with respect to H. The permeability is then given by

$$\mu = \frac{B}{H} = \frac{B_0 e^{i(\omega t - \delta)}}{H_0 e^{i\omega t}} = \frac{B_0 e^{-i\delta}}{H_0} = \frac{B_0}{H_0}\cos\delta - i\frac{B_0}{H_0}\sin\delta \tag{2.9}$$

$$\mu = \mu' - i\mu'' \tag{2.10}$$

Where $\mu' = \frac{B_0}{H_0}\cos\delta$ (2.11)

$$\mu'' = i\frac{B_0}{H_0}\sin\delta \quad (2.12)$$

The real Part μ' of complex permeability μ represent the component of B induction which is in phase with H, so it corresponds to the normal permeability. If there is no losses , we should have μ = μ', The imaginary part μ" corresponds to that part of B which is delayed by phase angle δ from H arranging up to 90° from H . The presence of such a component requires a supply of energy to maintain the alternating magnetization regardless of the origin of delay. The ratio of μ" to μ' as is evident from equation gives:

$$\frac{\mu'}{\mu''} = \frac{\frac{B_0}{H_0}\sin\delta}{\frac{B_0}{H_0}\cos\delta} = \tan\delta \quad (2.13)$$

This tan δ is called the loss Factor or loss tangent. The Q-Factor or quality factor is defined as the reciprocal of this loss factor, i.e.

$$Q = \frac{1}{\tan\delta} \quad (2.14)$$

And the relative quality factor = $\frac{\mu'}{\tan\delta} = \mu' Q$ (2.15)

The behavior of μ' and μ" versus frequency is called the permeability spectrum. The initial permeability of a ferromagnetic or ferromagnetic substance is the combined effects of the wall permeability and rotational permeability mechanisms.

2.7 Magnetization Process

A review of magnetization process, namely the response of ferro-or ferri magnetic material (bulk) to an applied field with a semi-microscopic approach is presented. In ferro- or ferri-magnetic material, the magnetization curves, especially in low magnetic fields differ widely from sample to sample and as a function of the magnetic history of the sample i.e., of the previous fields which have been successively applied.

2.7.1 Magnetization Curve

For unmagnetized bulk materials, there is a zero net magnetic moment. It can be predicted that there will be an infinite number of degree of magnetization between the unmagnetized and saturation conditions, when the material is subjected to an external magnetic field. These extreme situations are corresponds respectively to random orientation of domains complete alignment is one direction with elimination of domain walls. If we start with a demagnetized specimen and increase the applied magnetic field, the bulk material will progressively magnetized by the domain dynamics. The magnetization of the sample will follow the course as shown in figure 2.2 [2.16]. The slop from the origin to a point on the curve r the ratio MH is defined as magnetic susceptibility. This curve is called magnetization curve. This curve is generally perceived as being made of three major portions.

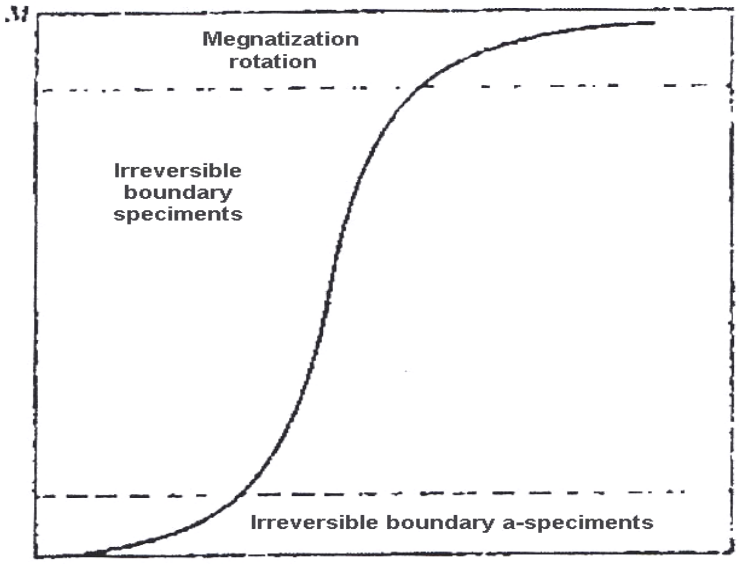

Figure 2.2: Domain dynamics during various parts of the magnetization curve

The first, the lower section, is the initial susceptibility region and characterized by reversible domain wall movements and rotations. By reversible means that after the magnetization slightly with an increase in field the origin magnetization can be reversed if the field is reduced to initial value. The condition of the displacement walls to an initial permeability is entirely dependent on the sort of material studied

In the second stage magnetization curve if the field is increased, the intensity of the magnetization increases more drastically is called the irreversible magnetization

range. This range is obtained mainly by the reversible domain wall motion from one stable state to another

If the field is increased further, the magnetization curve less step and its process become reversible once more. In the third section of magnetization curve, the displacement of domain walls have all ready been completed and the magnetizations take place by rotation magnetization. This range is called rotation magnetization range. Beyond this range the magnetization gradually approaches to saturation magnetization shown in figure 2.3

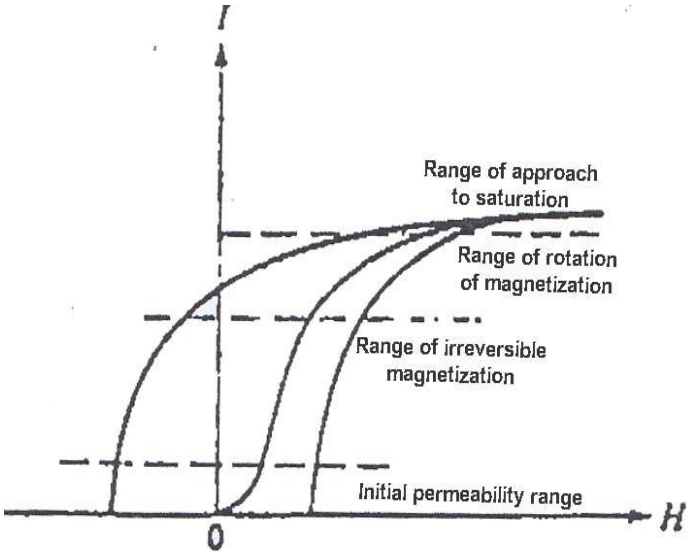

Figure 2.3: Magnetization curve and the classification of magnetization mechanism

2.8 DC Resistivity of Ferrites

Extensive investigation into the origin of the electrical conductivity of the spinels has been carried out by Verwey [2.17] and later on by Van Uitert [2.18] and Jonker [2.19]. The resistivity of ferrites at room temperature can vary, depending on chemical composition between about 10^{-2} to higher than 10^{+11} ohm-cm [2.8]. The low value of resistivity is due to the simultaneous presence of ferrous and ferric ions on equivalent lattice sites (octahedral) as proposed by Verwey [2.17]. For example Fe_3O_4 at room temperature has resistivity of approximately 7×10^{-3} Ohm-cm and Fe_2O_4 with some deficiency in iron and sintered in a sufficiently oxidizing atmosphere so that the product contains no ferrous ions can have a resistivity higher than 7×10^{6} ohm-cm. To make high resistivity ferrites one must sure that there are no ferrous ions in the stoichiometric ferrites.

Temperature dependent resistivity of ferrites follows Arrhenius relation [2.19]:

$$\rho = \rho_0 e^{\frac{E_a}{kT}}, \tag{2.16}$$

Where ρ is the resistively and E_a is the activation energy required for hopping of an electron from one lattice site to another.

2.9 Microstructure

A polycrystal is much more than many tiny crystals bonded together. The interfaces between the crystals, or the grain boundaries which separate and bond the grains, are complex and interactive interfaces. The whole set of a given material's properties (mechanical, chemical and especially electrical and magnetic) depend strongly on the nature of the microstructure. In the simplest case, the grain boundary is the region, which accommodates the difference in crystallographic orientation between the neighboring grains. For certain simple arrangements, the grain boundary is made of an array of dislocations whose number and spacing depends on the angular deviation between the grains. The ionic nature of ferrites leads to dislocation patterns considerably more complex than in metals, since electrostatic energy accounts for a significant fraction of the total boundary energy [2.20].

For low-loss ferrite, Ghate [2.20] states that the grain boundaries influence properties by

(i) Creating a high resistivity intergranular layer,

(ii) Acting as a sink for impurities which may act as a sintering aid and grain growth modifiers,

(iii) Providing a path for oxygen diffusion, which may modify the oxidation state of the cations near the boundaries.

In addition to grain boundaries, ceramic imperfections can impede domain wall motion and thus reduce the magnetic property. Among these are pores, cracks, inclusions, second phases, as well as residual strains. Imperfections also act as energy wells that pin the domain walls and require higher activation energy to detach. Stresses are micro structural imperfections that can result from impurities or processing problems such as too rapid a cool. They affect the domain dynamics and are responsible for a much greater share of the degradation of properties than would expect.

Grain growth kinetics depends strongly on the impurity content. A minor do pant can drastically change the nature and concentration of defects in the matrix, affecting grain boundary motion, pore mobility and pore removal [2.21]. The effect of a given do pant depends on its valence and solubility with respect to host material. If it is not soluble at the sintering temperature, the do pant becomes a second phase which usually segregates to the grain boundary.

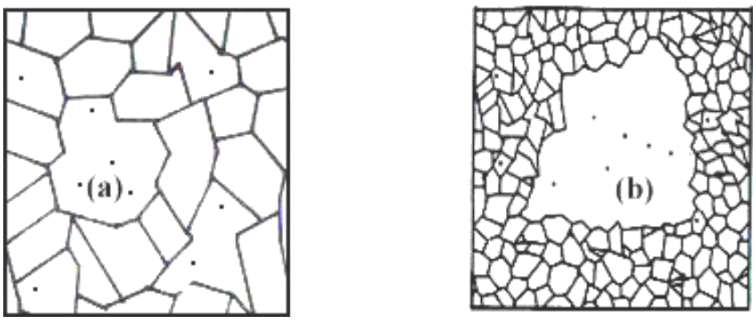

Figure 2.4: Porosity character: (a) intergranular, (b) intragranular

The porosity of ceramic samples results from two sources, intragranular porosity and intergranular porosity, figure 2.4. An undesirable effect in ceramic samples is the formation of exaggerated or discontinuous grain growth which is characterized by the excessive growth of some grains at the expense of small, neighboring ones, figure 2.5. When this occurs, the large grain has a high defect concentration. Discontinuous growth is believed to result from one or several of the following: powder mixtures with impurities; a very large distribution of initial particle size; sintering at excessively high temperatures; in ferrites containing Zn and /or Mn, a low O^2 partial pressure in the sintering atmosphere. When a very large grain is surrounded by smaller ones, it is called 'duplex' microstructure.

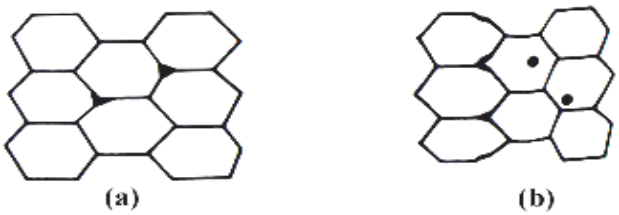

Figure 2.5: Grain growth (a) discontinuous, (b) duplex (schematic).

Experimental Procedure

3.1 Methodology of Rare Earth Ferrite Preparation

This chapter focuses on the methods and techniques used to synthesize, characterization and investigation of Mn-Zn based substituted mixed ferrites. Ferrites are ceramic compounds like Fe_2O_3 as their principal components. The spinel structure is the common form of all ferrites. Now-a-day, majority of ferrite powders are made by standard ceramic technique or solid state reaction methods are known as sintering. Many techniques have been developed for the improvements of the basic operations of ceramic fabrication. The preparation of rare earth ferrites with optimum desired properties is still a complex and difficult task. Knowledge and control of the chemical composition, homogeneity and microstructure are very crucial. The rare earth ferrite is not completely defined by its chemistry and crystal structure but also requires knowledge and control of parameters of its microstructure such as density grain size, porosity and their intra and intergranular distribution. It is well known that almost all rare earth ferrites decompose at the elevated temperature of we want to melt them under normal conditions. This happens because the oxygen splits off at higher temperature reducing Fe^{3+} and Fe^{2+}. This necessarily implies that ferrite preparation by melting as in case of metals is not possible. The normal methods of preparation of ferrites comprise of the conventional ceramic method or powder metallurgy chemical co-precipitation method and sol-gel method.

In this work conventional ceramic method has been employed for the preparation of $Mn_{0.5}Zn_{0.5}Y_xFe_{2-x}O_4$ ferrites for its relative simplicity and availability. The excellent powder preparation process and sintering facility available at the Solid State Physics Laboratory, KUET, Khulna has been utilized for the preparation of samples.

3.1.1 Compositions of the Studied Ferrites

A series of mixed ferrites of various compositions were prepared by solid state reaction technique keeping in view of their ionic radial and valences for maintaining the charge neutrality. In the present research, several compositions of Y substituted Mn-Zn soft ferrites are synthesized, characterized and investigated. The ferrites under investigation of composition $Mn_{0.5}Zn_{0.5}Y_xFe_{2-x}O_4$ where [x = 0.00, 0.02, 0.04, 0.06, 0.08 and 0.10].

3.1.2 Sample Preparation Technique

Structural and magnetic properties of rare earth substituted Mn-Zn ferrites are greatly dependent on fabrication technique. There are various fabrication processes. Single crystals of Y_2O_3 based dilute magnetic composition can be grown using chemical reaction. The most common methods for fabricating Yttrium oxide based diluted magnetic composition are given below:

The sample fabrication technique:

(i) Solid state reaction technique.

(ii) Bulk ZnO ion implantation.

(iii) Chemical solution method.

The ferrites of different compositions were prepared using ceramic technique involving solid state reaction from metal oxides MnO, ZnO, Y_2O_3, Fe_2O_3, in the form of grained powder having 99.99%. Different oxides were weighted precisely according to their molecular weight. The weight percentage of oxide to be mixed for various samples was calculated by using formula. The appropriate weight percentage of each oxide to be mixed for different composition by the following formula:

$$\text{Weight \% of oxide} = \frac{Molecular\ \ weigh\ \ of\ \ oxide \times required\ \ weight\ \ of\ \ the\ sample}{Sum\ of\ \ molecular\ \ weight\ \ of\ \ each\ oxide\ in\ a\ sample}$$

The calculated weight of oxide materials, molecular weight of oxides and wt.% calculated for each sample prepared are used for experiments.

3.1.3 Material synthesis and sample preparation

Most of the fabrication processes of diluted magnetic composition need many critical conditions to maintain and the maintenance of critical condition makes the fabrication process expensive. Among all the processes the solid state reaction process is relatively less expensive. Maintenance of the critical conditions here is relatively easier than other processes. Other advantages of this technique are reproducibility, easy control, and obtaining sufficient products for measurements. With a careful control of contamination and impurity, it is possible to fabricate a perfect dilute magnetic composition. The detail of the fabrication technique is described in the following section.

Polycrystalline $Mn_{0.5}Zn_{0.5}Fe_{2-x}Y_xO_4$ (X = 0.00, 0.02, 0.04, 0.06, 0.08 and 0.10) were prepared by standard solid state reaction technique. Appropriate amount of

commercially available high purity powders of $MnCO_3$ (99.9%), ZnO (99.9%), Y_2O_3 (99.95%) and Fe_2O_3 (99.9%) were used as the raw materials. The exact amounts of compounds were calculated for each composition. Using those raw materials were weighed and mixed thoroughly by hand milling. During hand milling, few drops of acetone were added to increase the degree of mixing. The mixture was calcined at 700ºC for 3 hours. The calcined powder again was crashed into fine powders. From the fine powders, toroid and disk-shaped samples were prepared and sintered at temperatures (1200^0C). During sintering the samples were heated /cooled in different heating and cooling rates. It was expected that sintering temperatures are produced samples of various surface morphology, electric and magnetic properties. The steps involving preparation of pellet or disc shaped and toroid shaped samples are described in following sections.

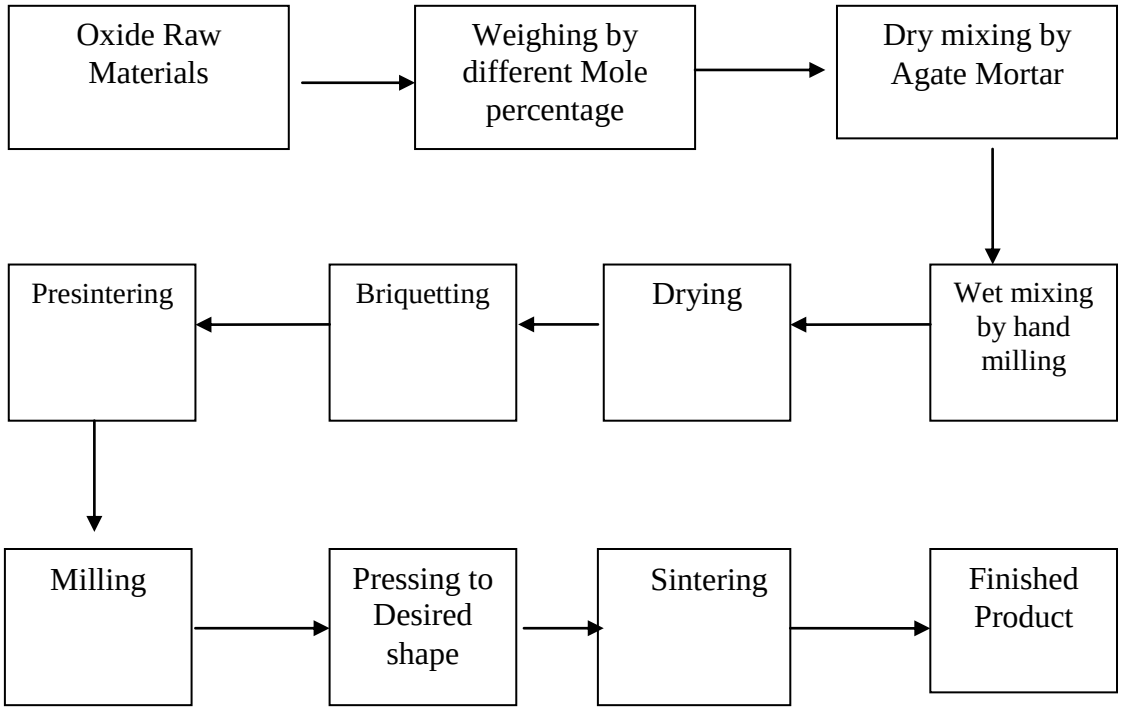

Figure 3.1: Flow chart of ferrite preparation.

The normal methods of preparation of ferrites comprise of the conventional ceramic method i.e. solid state reaction method involving hand milling of reactions following by sintering at elevated temperature range and non-conventional method, also called wet method chemical co-precipitation method and sol-gel method etc examples of wet method. The general preparation procedure of ferrites comprises of

the following operation as shown in figure 3.1. The block diagram and the detail of which are described subsequently.

3.2 Solid State Reaction Method

In the solid state reaction method, the required composition is usually prepare from the appropriate amount of raw mineral oxides or carbonates by crushing, grinding and milling [3.1]. Solid state reaction occurs between apparently regular crystal lattices, in which the kinetic motion is very much restricted and it depends on the presence of lattice defects [3.2]. In solid state reaction method, appropriate amounts of two or more component of chemical compounds are carefully grinded together and mixed thoroughly in mortar with pestle or ball milling with appropriate homogenization. Solid oxides do not usually react together at room temperature over normal time scale and it is necessary to heat them at much higher temperatures. The ground powders are then calcined in air or oxygen at a temperature above 700°C. Sometime this process is continued until the mixture is converted into the correct crystalline phase. The calcined powders are then further crushed into fine powders. The pellets or disc shaped and toroid shaped samples are made of these calcined powders using uniaxial or iso-static pressure. Sintering is carried out in the solid state, at temperatures between 700 - 1600°C, for times of typically 1- 5 hours and in various atmospheres (e.g. Air, O_2 and N_2)

The overall preparation process generally comprised of the following four major steps:

(i) Preparing a mixture of desired composition

(ii) Pre sintering the mixture to form ferrite

(iii) Converting the Raw ferrite into powder and pressing the powder

(iv) Sintering.

3.2.1 Preparing a Mixture of Materials

The extend of this work in these step greatly, depending on the starting materials, when component oxide are used, the corresponding step involves a mere mixing of the oxides by wet milling. To avoid iron contamination, mixing is done hand milling and a fluid such as distilled water is used to prepare the mixture into slurry. Ferric oxide, Fe_2O_3 and whatever oxides, MO are required are taken in powder form with the captions in the ratio corresponding to that in the final product. Metal

carbonate may also be used; during the later firing, CO_2 will be given off and they will be converted to oxides.

3.2.2 Pre-sintering the Mixture to Form Ferrite

The slurry prepared in step-1 is dried, palletized and then transferred to a porcelain crucible for pre sintering in a constant temperature of 700°C for 3 hours. Presintering of the materials was performed in a furnace named KSL-1700X FURNACE at Solid State Physics Laboratory, KUET, Khulna. The cooling and heating rates were 4°C/min. The pre-sintering is very crucial because in this step of sample preparation of ferrite is form its component oxides. The solid-state reactions, leading to the formation of ferrites, actually achieved by counter diffusion. This means that the diffusion involves two or more species of ions, which more in opposite direction initially across the interface of two contacting particles of different component oxides.

The ferrite is formed essentially in the pre-sintering step but the 'raw' ferrite formed has poor quality. In order to produce chemically homogeneous, dense and magnetically better material of desired shape and size, sintering at an elevated temperature is needed.

3.2.3 Converting the Raw Ferrite into Powder and Pressing the Powder

Besides reducing the particle size to ≈1micron, grinding also eliminates intra particle pores and homogenizes the ferrite by mixing. To promote successful sintering in the next steps, the powder must be well characterized after grinding with respect to such factors as particles size and distribution, particle shape, homogeneity, absorbed gases, impurities and intra particle porosity. Iron contamination due to continuous wear of the mill wall and steel ball need to be closely watched and minimized. Now to the ground homogeneous powder polyvinyl alcohol is added as a binder.

Pressing the powder into compacts of desired shapes is done either by conventional method in a die-punch assembly or by hydrostatic or isocratic compaction. We made use of the former one. Pressing a uniformly dense body by this method is difficult owing to the friction gradient of the powder at the walls of the die and between the particles themselves. This problems is somewhat overcome by the addition of external and internal lubricant to the powder such as stearic acid. Mainly, we made two types of samples- tablet and toroidal. Specimen was prepared by a

hydraulic press with a pressure of 1.5 ton/cm^2. The die was designed and made in the workshop of AECD. This is made of nonmagnetic stainless steel.

Figure 3.2: Hydraulic press used to make different shaped samples

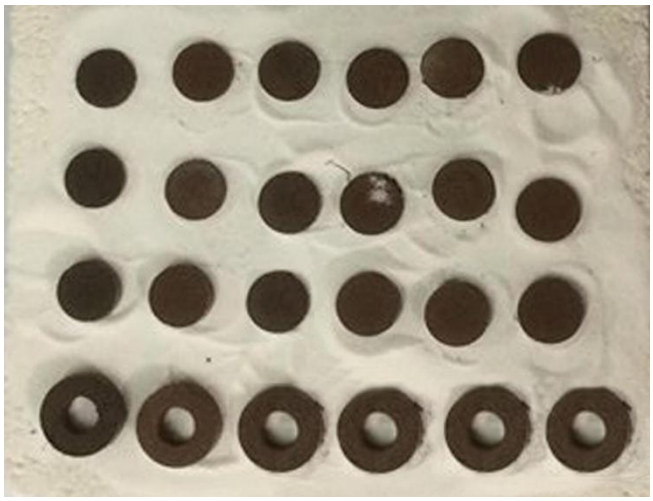

Figure 3.3: Toroid and disk shape sample

These oxide mixtures were milled thoroughly for 4-6 hours to obtain homogeneous mixture. The mixture was dried and a small amount of saturated solution of polyvinyl alcohol (PVA) were added as a binder and pressed into pellet and toroid shape respectively under pressure 1.75 ton-cm^{-2} and 1.2 ton-cm^{-2} using hydraulic press figure 3.2. The prepared samples shown in figure 3.3 were sintered at

1200°C for 2hrs with a microprocessor controlled muffle furnace. The samples were polished in order to remove any oxide layer formed during the process of sintering.

3.2.4 Sintering

Powder sintering involves raising the temperature of the green compact, (pressed powder part), to a certain level and keeping it at that temperature for a certain amount of time. The sintering temperature is usually between 70% and 90% of the melting point of the powder metal. This will cause bonding mechanisms to occur between powder particles pressed together in the compact. Bonding within the green compact is weak and this pressed unsintered part usually has just enough structural integrity to be handled. Bonding that occurs during sintering greatly strengthens the part.

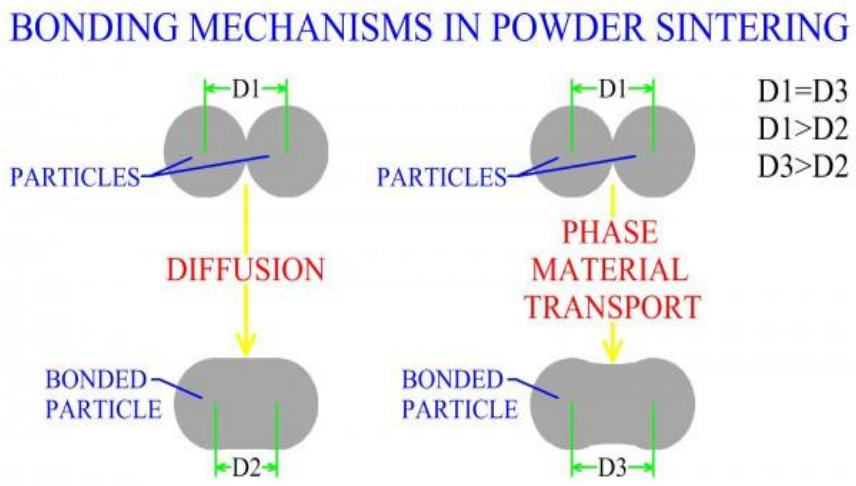

Figure 3.4: Bonding Mechanism in Powder Sintering.

Sintering involves heating the powdered metal compacts in vacuum or a reducing gaseous atmosphere to a temperature that is below the melting point of the primary constituent of the material. The metallic particles metalurgically bond and alloying take place via diffusion processes. Changes occur during sintering, including changes in size, configuration, and the nature of pores (figure 3.4). Commonly used atmospheres for sintering are hydrogen, carbon monoxide, and ammonia. Sintering operation ensures that powder particles are bonded strongly and that better alloying is achieved [3.3].

This is a heat treatment by which a mass of compacted powder is transformed into a dense object. The thermodynamic driving force is the reduction in the specific

surface area of the particles. The sintering mechanism usually involves atomic transport over particle surfaces, along grain boundaries and through the particle interiors. Sintering may result in densification, depending on the predominant diffusion pathway. It is used in the fabrication of metal and ceramic components, the agglomeration of ore fines for further metallurgical processing and occurs during the formation of sandstones and glaciers. Sintering must fulfill three requirements

- to bond the particles together so as to impart sufficient strength to the product
- to density the grain compacts by eliminating the pores and
- To complete the reactions left unfinished in the pre-sintering step.

Figure 3.5: Furnace used in solid state Physics lab of KUET

The principle goal of sintering is the reduction of compact porosity. Sometimes the initial spaces between compacted grains of ceramics are called “voids”, to differentiate term from the isolated spaces pores, which occur in the final stages of sintering. The sintering process is usually accompanied by other changes within the materials, some desirable and some undesirable. The largest- changes occur in:

- Binding the particles together so as to impart sufficient strength to the products.
- Densification the green compacts by eliminating the pores.

- Making strength of elastic modulus
- Making homogeneous distribution of grain number, grain size and shape.
- Developing the average pore size and shape.

Sintering can be enhanced by the presence of a liquid phase. The liquid phase can form directly from the elements when the sintering temperature is between the melting point of the matrix and the additive, by the melting of eutectic phase mixtures, which form by diffusion or by incipient melting. The liquid flows between the particles filling pores and causing densification by capillary action and through the provision of a fast diffusion pathway.

3.3 X-ray Diffraction (XRD)

The peaks in an X-ray diffraction pattern are directly related to the atomic distance. Let us consider an incident X-ray beam interacting with the atoms arranged in a periodic manner as shown in two dimensions in figure 3.6. The atoms, represented as spheres in the illustration, can be viewed as forming different sets of planes in the crystal. For a given set of lattice planes with an inter-plane distance of d, the condition for a diffraction (peak) to occur can be simple written as

$$2d \sin n\theta = n\lambda \ , \tag{3.1}$$

which is known as Bragg's law. In the equation, λ is the wavelength of the X-ray, θ is the scattering angle, and n is an integer representing the order of the diffraction peak. The Bragg's Law is one of the most important laws used for interpreting X - ray diffraction data. From the law, we find that the diffraction is only possible when λ < 2d [3.4].

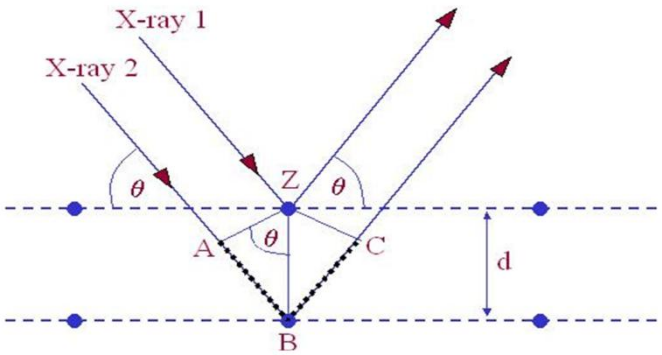

Figure 3.6: Bragg's diffraction pattern

In the present work, A PHILIPS PW 3040 X'pert PRO X-ray diffractometer was used for the lattice parameter to study the crystalline phases of the prepared

samples in the Materials Science division, Atomic Energy Centre, Dhaka. Figure 3.8 shows the block diagram of X'pert PRO XRD system. The powder diffraction technique was used with a primary beam powder of 40 kV and 30mA for Cu-K_α radiation. A nickel filter was used to reduce Cu-K_β radiation and finally Cu-K_α radiation was only used as the primary beam. The experimental has been performed at room temperature. A 2θ scan was taken from 15° to 75° to get possible fundamental peaks of the samples with the sampling pitch of 0.02° and time for each step data collection was 1.0 sec. Both the programmable divergence and receiving slits were used to control the irradiated beam area and output intensity from the powder sample, respectively. An anti scatter slit was used just after the tube and in front of the detector to get parallel beam only. All the data of the samples were stored in the computer memory and later on analyzed them using computer "software, X' PERT HJGHS CORE". For XRD experiment each sample was set on a glass slide and fixed the sample by putting adhesive typed the two ends of the sample.

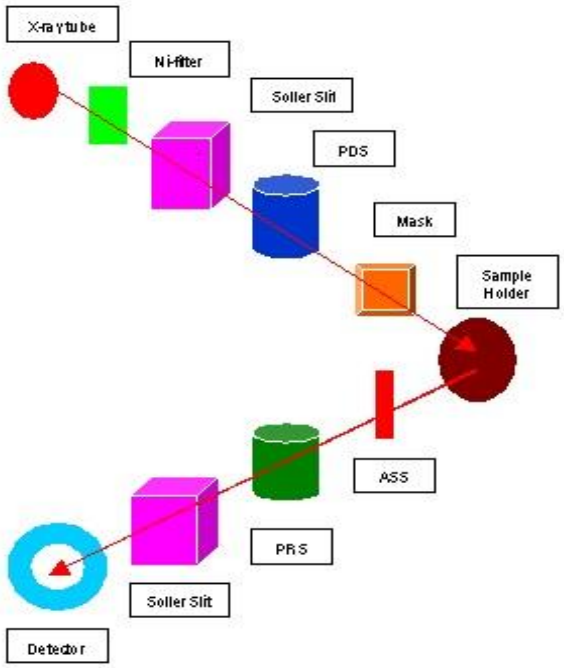

Figure 3.7: Block diagram of the PHILIPS PW 3040 X' Pert PRO XRD system

For each composition, the cylindrical samples of weight more than 2 gm are converted into powder. For XRD experiment each sample was set on a glass slide and fixed the sample by putting adhesive tape at the two ends of the sample X-ray diffraction patterns were carried out to confirm the crystal structure. Instrumental broadening of the system was determined from θ–2θ scan of standard Si. At (311)

reflection's position of the peak, the value of instrumental broadening was found to be 0.07°. This value of instrumental broadening was subtracted from the pattern. After that, using the X-ray data, the lattice constant (a) and hence the X-ray densities were calculated.

3.3.1 Different Parts of the PHILIPS X' Pert PRO XRD System

Figure 3.9 shows the inside view of the X' pert PRO XRD system. A complex of instruments of X- ray diffraction analysis has been established for both materials research and specimen characterization.

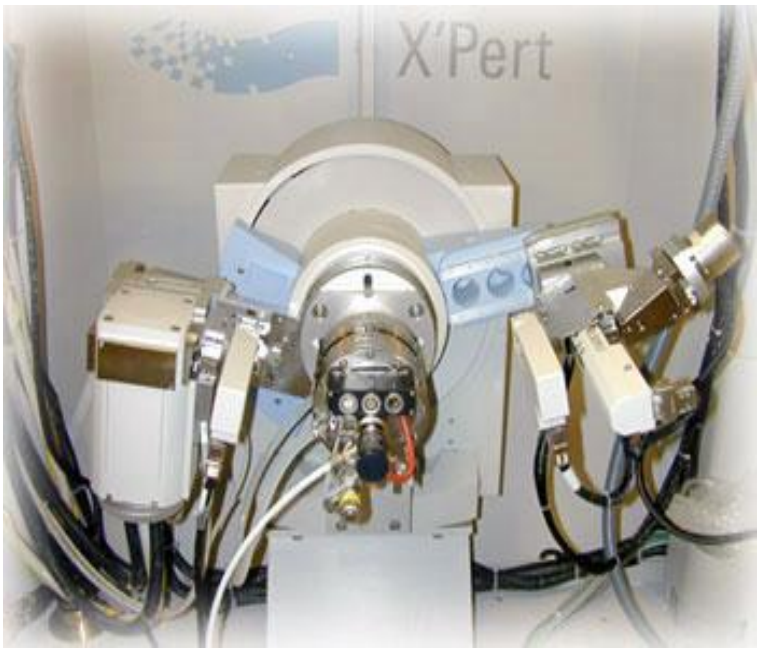

Figure 3.8: Internal arrangement of a PHILIPS X' Pert PRO X-ray diffractometer

These include facilities for studying single crystal defects, and a variety of other materials problems.

The PHILIPS X' Pert PRO XRD system comprised of the following parts;

(i) Cu-Tube with maximum input power of 60 kV and 55 mA,

(ii) Ni- Filter to remove Cu-K_α component,

(iii) Solar slit to pass parallel beam only,

(iv) Programmable Divergent slits (PDS) to reduce divergence of beam and control irradiated beam area,

(v) Mask to get desired beam area,

(vi) Sample holder for powder sample,

(vii) Anti Scatter slit (ASS) to reduce air scattering back ground,

(viii) Programmable Receiving slit (PRS) to control the diffracted beam intensity and

(ix) Solar slit to stop scattered beam and pass parallel diffracted beam only.

3.3.2 Interpretation of the XRD data

The XRD data consisting of θ_{hkl} and d_{hkl} values corresponding to the different crystallographic planes are used to determine the structural information of the samples like lattice parameter and constituent phase. Lattice parameters of Co-ferrites samples were determined. Normally, lattice parameter of an alloy composition is determined by the Debye-Scherrer method after extrapolation of the curve. We determine the lattice spacing (interplaner distance), d using these reflections from the equation which is known as Bragg's Law.

$$2d_{hkl}\,\mathrm{Sin}\theta = \lambda$$

$$\text{i.e. } d_{hkl} = \frac{\lambda}{2\sin\theta}\ , \qquad (3.2)$$

where λ is the wavelength of the X-ray, θ is the diffraction angle and n is an integer representing the order of the diffraction.

3.3.3. Lattice Parameter

The lattice parameter for each peak of each sample was calculated by using the formula:

$$a = d_{hkl} \times \sqrt{h^2 + k^2 + l^2}\ , \qquad (3.3)$$

where h, k, l are the indices of the crystal planes. We get d_{hkl} values from the computer using software "X' Pert HJGHS CORE". So we got ten 'a' values for ten reflection planes such as a a_1 , a_2 a_3 ….. etc. Determine the exact lattice parameter for each sample, through the Nelson-Riley extrapolation method. The values of the lattice parameter obtained from each reflected plane are plotted against Nelson-Riley function [3.4].The Nelson-Riley function F (θ), can be written as

$$F(\theta) = \frac{1}{2}\left[\frac{\cos^2\theta}{\sin\theta} + \frac{\cos^2\theta}{\theta}\right], \qquad (3.4)$$

where θ is the Bragg's angle. Now drawing the graph of 'a' vs. F(θ) and using linear fitting of those points will give us the lattice parameter 'a_0'. This value of 'a_0' at F(θ) = 0 or θ = 90° .These 'a_0's are calculated with an error estimated to be ± 0.0001Å.

3.3.4 X-ray Density and Bulk Density

X-ray density, d_x was also calculated usual from the lattice constant. The relation between d_x and 'a' is as follows,

$$d_x = \frac{ZM}{Na^3} \tag{3.5}$$

where M is the molecular weight of the corresponding composition, N is the Avogadro's number ($6.023X10^{23}$ $mole^{-1}$), 'a' is the lattice parameter and Z is the number of molecules per unit cell, (Z = 8 for the spinel cubic structure). The bulk density was calculated considering a cylindrical pellet of mass (m) and volume (V) of the pellets using the relation

$$d_B = \frac{m}{V} = \frac{m}{\pi r^2 h}, \tag{3.6}$$

where m is the mass of the pellet sample, r is the radius and h is the thickness of the pellet.

3.3.5 Porosity

Porosity is a parameter which is inevitable during the process of sintering of oxide materials. It is noteworthy that the physical and electromagnetic properties are strongly dependent on the porosity of the studied samples. Therefore an accurate idea of percentage of pores in a prepared sample is prerequisite for better understanding of the various properties of the studied samples to correlate the microstructure property relationship of the samples under study. The porosity of a material depends on the shape, size of grains and on the degree of their storing and packing. The difference between the bulk density d_B and X-ray density d_x gave us the measure of porosity. Percentage of porosity has been calculated using the following relation [2.19]

$$P = (1 - \frac{d_B}{d_x}) \times 100\% \tag{3.7}$$

3.4 Permeability Measurement

3.4.1 Wayne Kerr Precision Impedance Analyzer

The Wayne Kerr Technologies 6500B impedance analyzer greatly supports accurate impedance measurement and analysis of a wide variety of electronic devices (components and circuits) as well as electronic and non-electronic material Fig: 3.10. We made use of the excellent experimental facilities available at the Solid State Physics Laboratory, KUET, Khulna. Moreover, the 6500B"s high measurement

performance and capable functionally delivers a powerful tool to circuit design and development as well as materials research and development (both electronic and non electronic materials) environments:

- Accurate measurement over wide impedance range and wide frequency range.
- Powerful impedance analysis functions.
- Ease of use and versatile PC connectivity.

The following are application examples:

- Impedance measurement of two terminal components such as capacitors, inductors, ferrite beads, resistors, transformers, crystal / ceramic resonators, multi-chip modules or array/network components

Semiconductor components:

- C – r characteristic analysis of varac for diodes.
- Parasitic analysis of a diode, transistor or IC package terminal/leads.
- Amplifier input/output impedance measurement
- Impedance evaluation of printed circuit boards, relays, switches, cables, batteries etc.

Dielectric materials: Permittivity and loss tangent evaluation of plastics, ceramics, printed circuit boards and other dielectric material.

Magnetic materials : Permeability and loss tangent evaluation of ferrite, amorphous and other magnetic materials.

Semiconductor material: Permittivity, conductivity and C–V characteristics of semiconductor materials.

3.4.2 Permeability

From the frequency dependence of complex permeability, evolution of permeability and magnetic loss component at different stages of ferrite sample as affected by thermal treatment at different temperature was determined using toroids shape sample prepared with insulating Cu wire. The WK 6500B Impedance analyzer directly measures the value of inductance as shown in figure 3.10, L and loss factor.

$$D = \tan\delta \tag{3.8}$$

From inductance the value of real part of complex permeability, μ' can be obtained by using the relation

$$\mu' = \frac{L}{L_0} \ , \tag{3.9}$$

where L is the inductance of the toroid and L_o is the inductance of the coil of same geometric shape in vacuum, L_o is determined by using the relation,

$$L_0 = \frac{\mu_0 N^2 S}{\pi \bar{d}} \tag{3.10}$$

Figure 3.9: Impedance Analyzer Model-Wayne kerr,6500B

Here μ_o is the permeability of the vacuum, N is the number of turns (here N = 8), S is the cross-sectional area of the toroid shaped sample, S = dh, where,

$d = \frac{d_1 \sim d_2}{2}$ and $\bar{d}$ is the average diameter of the toroid sample given as

$$\bar{d} = \frac{d_1 + d_2}{2} \ , \tag{3.11}$$

where, d_1 and d_2 are the inner and outer diameter of the toroid samples.

3.5 Magnetization Measurement Techniques

Magnetization in ferrite samples originate due to the difference in the magnetic moments for the two sub-lattices. The larger the difference, the greater is the resultant magnetization, because of the anti-parallel arrangements of the moments in two sub-lattices. The magnetic moment of each sub-lattice arises due to the presence of magnetic ions such as Fe^{2+}, Fe^{3+}, Mn^{2+}, Cu^{2+}, Ni^{2+}, Co^{2+} etc. In our case, only iron ion has magnetic moment since Mn and Zn are non-magnetic. Different ions occupy

different 2 sites. So, as a whole, the two sub-lattices have their individual resultant magnetic moments. The differences in magnetic moment between the two sub-lattices give rise to net magnetic moment which in turn yields magnetization. In the present study magnetization has been performed using a VSM.

3.5.1 Vibrating Sample Magnetometer of Model EV7 System

The principle of VSM is the measurement of the electromotive force induces by magnetic sample when it is vibrate at a constant frequency in the presence of a static and uniform magnetic field. A small part of 10-50mg was weighed and made to avoid movements inside the sample holder

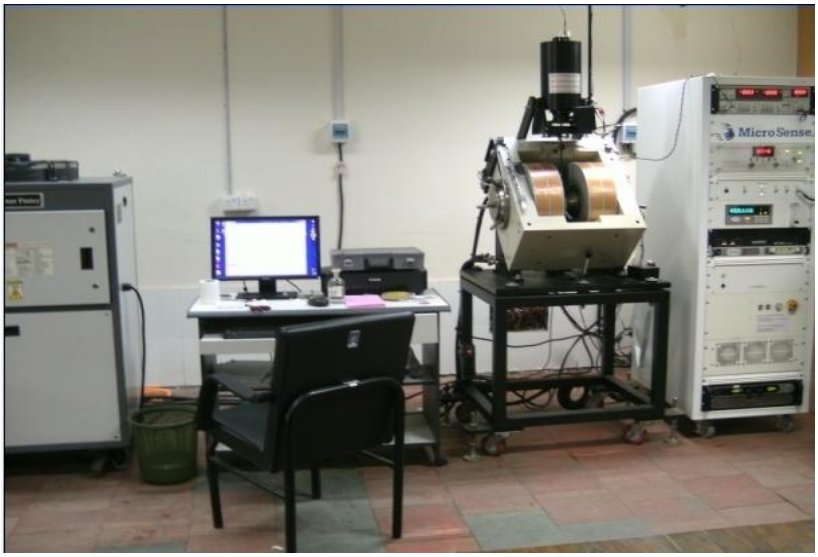

Figure 3.10: Vibrating Sample Magnetometer

The magnetic properties measurement system Model EV7 is a sophisticated analytical instrument configured specially for the study of the magnetic properties of small samples over a broad range of temperature from 103K to 800k and magnetic field from-20KOe to +20KOe. Vibrating Sample Magnetometer is a versatile and sensitive method of measuring magnetic properties developed by S. Foner [3.5] and is based on the flux change in a coil when the sample is vibrated near it.

The VSM is designed to continuously measure the magnetic properties of materials as a function of temperature and field. In this type of magnetometer, the sample is vibrated up and down in a region surround by several pickup coils. The magnetic sample is thus acting as a time-changing magnetic flux, varying magnetic flux is accompanied by an electric field and the field induces a voltage in pickup coils. This alternating voltage signal is processed by a control unit system, in order to

increase the signal to noise ratio. The result is a measure of the magnetization of the sample.

3.6 Surface morphology and microstructure

The microstructural study was performed in order to have an insight of the grain structures. The samples of different compositions and sintered at different temperatures were chosen for this purpose. The samples were visualized under a High-resolution SEM and then photographed. Average grain sizes (grain diameter) of the samples were determined from SEM micrographs by linear intercept technique [3.6]. To do this, several random horizontal and vertical lines were drawn on the micrographs. Therefore, we counted the number of grains intersected and measured the length of the grains along the line traversed. Finally the average grain size was calculated.

3.6.1 Scanning Electron Microscope (SEM)

SEM is a type of electron microscope that creates various images (surface morphology) by focusing a high energy beam of electrons onto the surface of a sample and detecting signals from the interaction of the incident electron with the sample's surface. The type of signals gathered in a SEM varies and can include secondary electrons, characteristic x-rays, and back scattered electrons. In a SEM, these signals come not only from the primary beam impinging upon the sample, but from other interactions within the sample near the surface. The SEM is capable of producing high resolution images of a sample surface in its primary use mode, secondary electron imaging. Due to the manner in which this image is created, SEM images have great depth of field yielding a characteristic three-dimensional appearance useful for understanding the surface structure of a sample. This great depth of field and the wide range of magnifications are the most familiar imaging mode for specimens in the SEM. Characteristic x-rays are emitted when the primary beam causes the ejection of inner shell electrons from the sample and are used to tell the elemental composition of the sample. The back-scattered electrons emitted from the sample may be used alone to form an image or in conjunction with the characteristic x-rays as atomic number contrast clues to the elemental composition of the sample. In the present study, the SEM micrographs of different sintered pellets

were taken using a field emission scanning electron microscope (FESEM, JEOL, JSM 7800F)

Figure 3.11: Scanning Electron Microscope (SEM)

3.6.2 Scanning process and image formation

In a typical SEM, an electron beam is thermionic ally emitted from an electron gun fitted with a tungsten filament cathode. Tungsten is normally used in thermo ionic electron guns because it has the highest melting point and lowest vapor pressure of all metals, thereby allowing it to be heated for electron emission, and because of its low cost. The electron beam, which typically has an energy ranging from a few 100 eV to 40 keV, is focused by one or two condenser lenses to a spot about 0.4 nm to 5 nm in diameter. The beam passes through pairs of scanning coils or pairs of deflector plates in the electron column, typically in the final lens, which deflect the beam in the x and y axes so that it scans in a raster fashion over a rectangular area of the sample surface.

The primary electron beam interacts with the sample, the electrons lose energy by repeated random scattering and absorption within a teardrop-shaped volume of the specimen known as the interaction volume, which extends from less than 100 nm to around 5 µm into the surface. The size of the interaction volume depends on the electron's landing energy, the atomic number of the specimen and the specimen's density. The energy exchange between the electron beam and the sample results in the reflection of high-energy electrons by elastic scattering, emission of secondary electrons by inelastic scattering and the emission of electromagnetic radiation, each of which can be detected by specialized detectors. The beam current

absorbed by the specimen can also be detected and used to create images of the distribution of specimen current. Electronic amplifiers of various types are used to amplify the signals which are displayed as variations in brightness on a cathode ray tube. The raster scanning of the CRT display is synchronized with that of the beam on the specimen in the microscope, and the resulting image is therefore a distribution map of the intensity of the signal being emitted from the scanned area of the specimen. The image may be captured by photography from a high resolution cathode ray tube, but in modern machines is digitally captured and displayed on a computer monitor.

3.7 Dielectric Properties

Ceramics are mostly covalently bonded material hence electrically non conductive or insulator. Importance of particular property depends on the application demand. For instance, dielectric strength is an important parameter for application of ceramic as insulators used in power transmission line, load bearing general insulators, in house hold appliances etc. In this kind of applications where frequency do not exceed 1kHz, the break down strength, measured in kV/cm, together with mechanical strength are important factors. The dielectric constant ($\varepsilon^{/}$) or loss factor ($\varepsilon^{//}$) does not matter much. On the other hand, for capacitors and electronics application just the opposite required. The values of $\varepsilon^{/}$ and $\varepsilon^{//}$ are of prime importance, not only their room temperature values but also as function of frequency. These are intrinsic properties of material; especially of polycrystalline ceramic can be modified by doping, micro structural variation.

3.7.1 Dielectric Constant

Dielectric constant measurements were done by using Wayne Kerr Impedance Analyzer 6500B. The overall dielectric constant ($\varepsilon^{/}$) of an insulator material as given by the relation:

$$D = \varepsilon_0 E = \varepsilon_0 \varepsilon' E \tag{3.12}$$

D represents the electric displacement, E the electric field in the dielectric, $\varepsilon^{/}$ the dielectric constant and ε_0 permittivity of the vacuum. The electric displacement describes the extent to which the electric field has been altered by the presence of the dielectric material. The dielectric constant $\varepsilon^{/}$ is an intrinsic property of a material and

a measure of the ability of the material to store electric charge relative to vacuum. It is measured directly from the capacitance of a capacitor in which the material is used as electrode separator or dielectric. The capacitive cell, the dielectric constant (ε'), total charge (q) and capacitance © can be developed as follows:

$$\varepsilon' = \frac{D}{\varepsilon_0 E} = \frac{\frac{Q}{A}}{\frac{\varepsilon_0 V}{d}} \tag{3.13}$$

$$\therefore Q = \frac{\varepsilon_0 \varepsilon' A V}{d} = CV \tag{3.14}$$

Where $C = \frac{\varepsilon_0 \varepsilon' A}{d}$ (3.15)

Here A represents the area of the capacitive cell, d its thickness, C is the capacitance of the material, V the voltage across the cell and $\varepsilon_0\left(\frac{F}{m}\right)$ the material permittivity in vacuum. Thus ε' represents the ratio of the permittivity or charge storage capacity relative to air or vacuum as dielectric.

$$\varepsilon' = \frac{cd}{\varepsilon_o A}, \tag{3.16}$$

where c is the capacitance of the pellet in Farad, d the thickens of the pellet in meter , A the cross-sectional area of the flat surface of the pellet in m^2 and ε_o the constant of permittivity for free space. Dielectric measurement as a function of frequency in the range 100Hz-13MHz at room temperature were carried out by using Wayne Kerr Impedance Analyzer 6500B in conjunction with a laboratory made furnace which maintain the desired temperature with the help of a temperature controller.

RESULTS AND DISCUSSION

4.0 Introduction

The polycrystalline spinel ferrites present an important set of properties such as high permeability in the radio frequency level, high electrical resistivity, low dielectric losses, low eddy current losses, low cost and environmental stability [4.1 – 4.3]. Ferrites are used today in radio and television, microwaves and satellite communications, audio, video and digital recording and as permanent magnets. The best quality video heads require ferrite cores which can show high permeability in its operating frequency band. Mn-Zn ferrites can be used as video heads. Thus, we believe that researches on ferrites are very important for Bangladesh perspective. Dilute $Mn_{0.5}Zn_{0.5}Fe_2O_4$ with non magnetic Zn and Mn content higher than percolation limit where frustration and competing interaction start to play dominant role has higher to not been studied in much detail. Some anomaly must be found for $Mn_{0.5}Zn_{0.5}Fe_2O_4$ ferrite because the ionic radii of substituted Zn^{2+} ion lower than Mn^{2+} ion. Now–a-days the rare earth oxides are becoming promising additives to change the magnetic properties of ferrites. The properties can be changed by substitutions various kinds of divalent cations or relatively small amount of rare earth ions [4.4]. The properties are very sensitive to preparation environment such as sintering temperature, time and type of additives [4.5]. The spinel ferrites having general formula $Mn_{0.5}Zn_{0.5}Y_xFe_{2-x}O_4$ where x = 0.00, 0.02, 0.04, 0.06, 0.08, 0.10 have been prepared by the standard solid state reaction method sintered at 1200 ºC for 2 hours. The effects rare earth ion Y^{3+} substitution on Mn-Zn ferrites are significant change in the structural, microstructure, permeability, magnetic loss, saturation magnetization, electrical resistivity and dielectric constant.

4.1 X-Ray Diffraction Analysis

X-ray neutron and electron diffraction are useful techniques to evaluate the various phases of the synthesized ferrites as well as their unit cell parameters. In the present study X-ray diffraction technique has been utilized to discern these parameters X-ray diffraction (XRD) studies of the samples were performed by using Philips PERT PRO X-ray Diffraction using Cu-K_α radiation in the range of $2\theta = 15^0$ to 65^0 in steps of 0.02^0. The Fe replaced Y substitution in base ferrite $Mn_{0.5}Zn_{0.5}Y_xFe_{2-x}O_4$ has

a significant influence on the structural and physical properties such as lattice constant, X-ray density, bulk density, porosity etc. The porosity was calculated from the X-ray density and bulk density. The possible experimental and theoretical reasons responsible for the change in substitution of the above mentioned properties have been discussed below.

4.1.1 Phase Analysis

XRD patterns of the sample $Mn_{0.5}Zn_{0.5}Y_xFe_{2-x}O_4$ ferrites where x = 0.00, 0.02, 0.04, 0.06, 0.08, 0.10 sintered at 1200^oC for 2 hours shown figure 4.1. The XRD patterns for all the samples were indexed for fcc spinel structure and Bragg diffraction planes are shown in the patterns. The structural model has been taken as the spinel phase. All the samples show good crystallization with well defined diffraction lines. It is obvious that the characteristic peaks for spinel ferrites i. e. (111), (220), (311),(222),(400),(422), (511) and (440), which represent either all odd or even indicating that the samples are spinel cubic phase. The single phase has been obtained $Mn_{0.5}Zn_{0.5}Fe_2O_4$ without any extra peak where as Y^{3+} doped samples how additional peaks other than spinel structure probably corresponding to second phase of $YFeO_3$ (Ortho ferrite) shown in figure 4.1.

However, a very weak reflection peak at $2\theta = 36.02^o$ is about to emerge for x = 0.02 – 0.10 is more prominent indicated by the arrow. This peak is identified as the weak reflection peak of the $YFeO_3$ phase. To identify the possible formation of a second phase $YFeO_3$ in the substituted ferrites, the slow step scan XRD analysis was conducted on the samples after different steps of processing. $YFeO_3$ phase was in all Y substituted ferrites in the replace of Fe. The amount of $YFeO_3$ that is peak intensity increased with increasing Y concentrations indicated by arrow. This apparently indicated that Y did not form a solid solution with spinel ferrites or it had very solid solubility.

Determination of exact phase could not be possible, since the number of extra peaks other than Spinel is not sufficient for accurate analysis. XRD analysis evidenced that the compounds containing Y^{3+} ions are pluri-phasic. Rare earth is formed orthoferrite ($YFeO_3$) phase and the formation of these secondary phases in ferrite during sintering process was governed by the type and the amount of Y^{3+} ions used. The lattice parameter ‘a’ corresponding to each plane was calculated by using

the X-ray data. The average values of 'a' were found by plotting a against Nelson-Riley function.

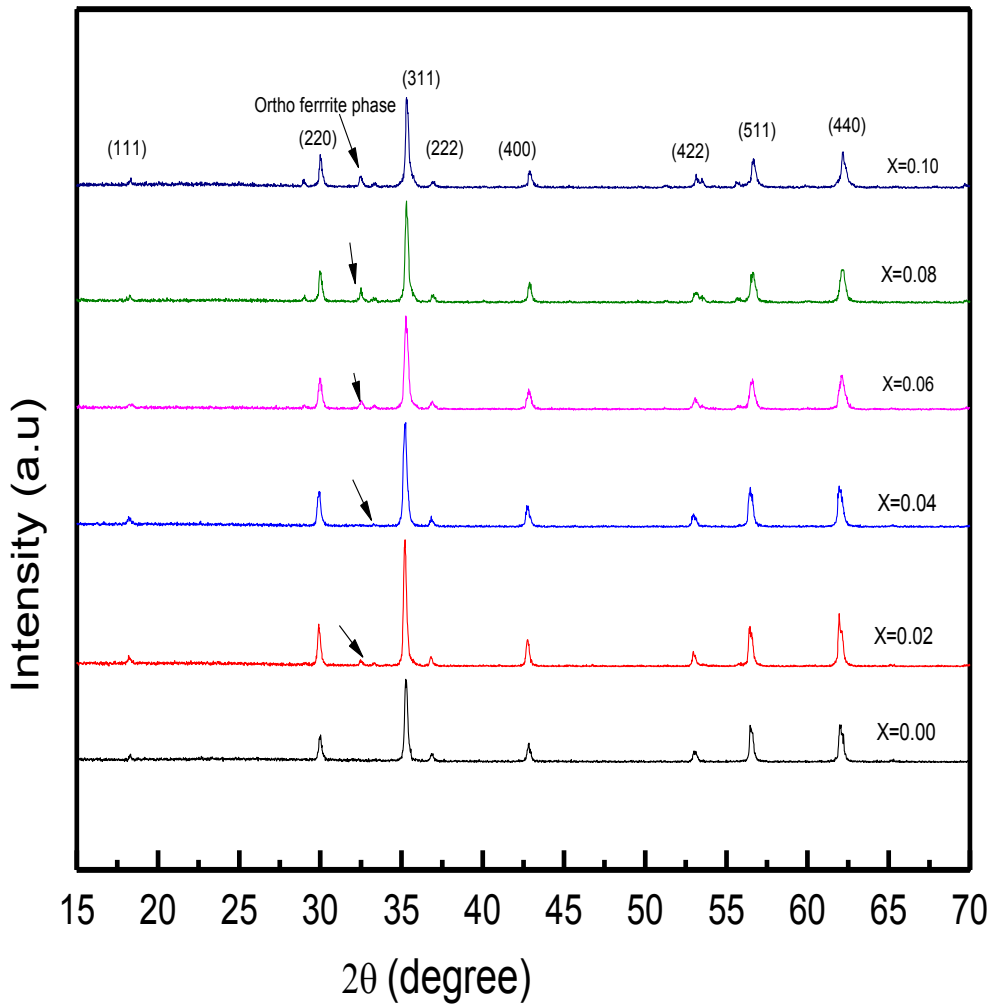

Figure 4.1: X-ray diffraction patterns of $Mn_{0.5}Zn_{0.5}Y_xFe_{2-x}O_4$ [x = 0.00, 0.02, 0.04, 0.06, 0.08 and 0.10] ferrites sintered at 1200^0C for 2hrs.

4.1.2 Lattice Parameters

The values of lattice parameters have been determined from each plane of XRD pattern using Nelson Relay function (4.6) $F(\theta)=\frac{1}{2}\left[\frac{Cos^2\theta}{Sin\theta}+\frac{Cos^2\theta}{\theta}\right]$ where θ is the Bragg's angle, by extrapolating lattice parameter's values of F (θ) = 0 or θ = 90^0. The lattice parameters are plotted against the Nelson Relay function, F (θ) shown in figure 4.2 (a – f) for Y content.

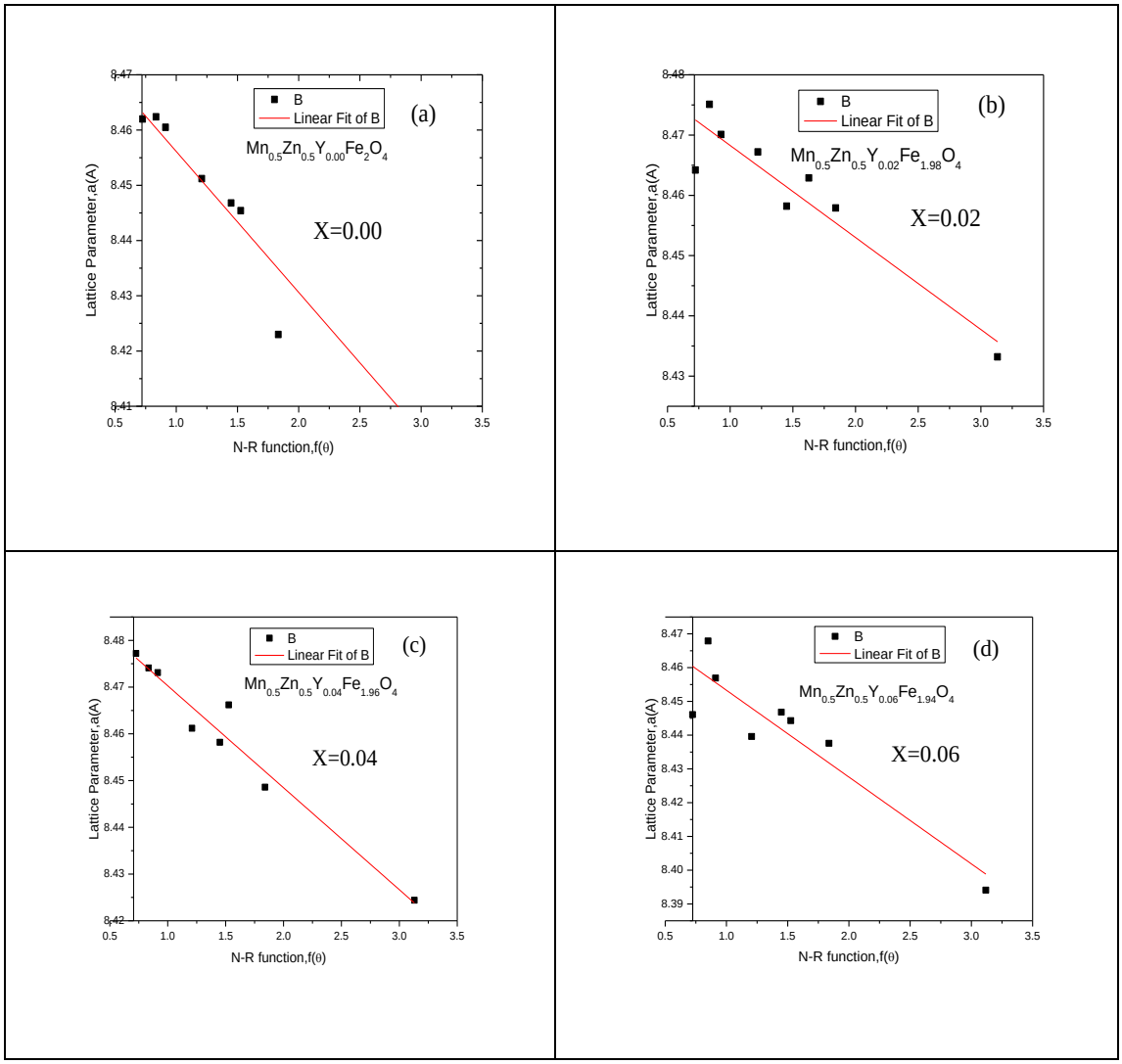

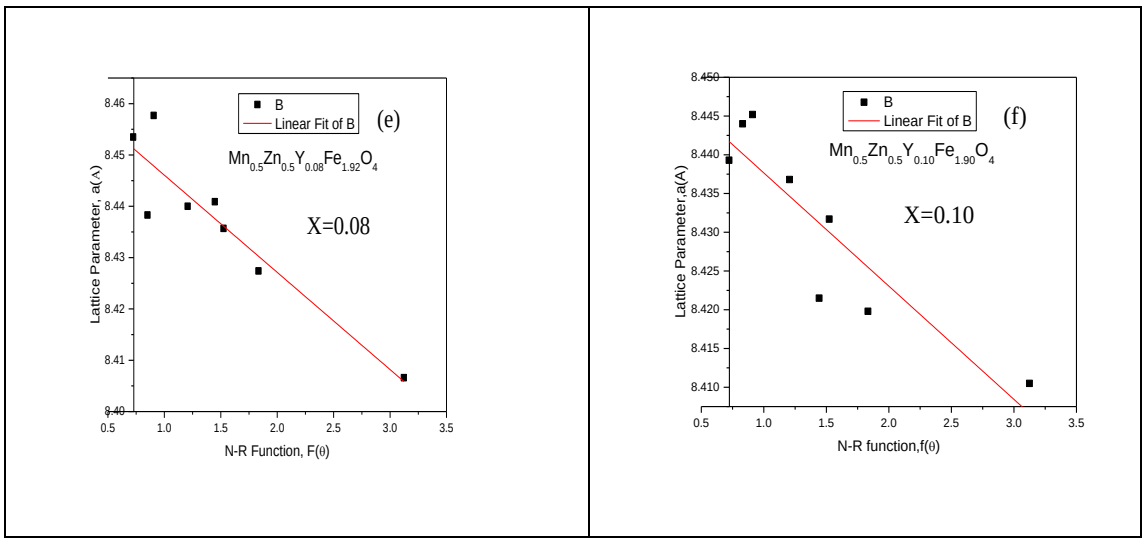

Figure 4.2 (a-f): Variation of lattice parameter 'a' with N - R function and determination of exact lattice parameter 'a_0' of $Mn_{0.5}Zn_{0.5}YxFe_{2-x}O_4$ [x = 0.00, 0.02, 0.04, 0.06, 0.08 and 0.10]

The lattice parameter (a_0) increases at x = 0.02 and 0.04 due the replacement of Fe^{3+} ions (radius = 0.64A^o) by the larger Y^{3+} ions (radius = 1.12A^o) in the octahedral sites shown in table 4.1. No significant decrease in 'a_0' is observed in the present experiment. There is a slight decrease Y^{3+} (radius = 0.90Å) in the octahedral sites, indeed, lattice parameter was in the same range of different. However, no significant decrease in 'a_0' is observed in the present experiment for x = 0.06, 0.08 and 0.10. The decrease in 'a_0' between x = 0.06, 0.08 and 0.10 is probably due to distortion in the spinel lattice because of the relatively large radius of Y^{3+} shown in table 4.1. This is evidenced by the appearance of the minor $YFeO_3$ phase at x = 0.06, 0.08 and 0.10.

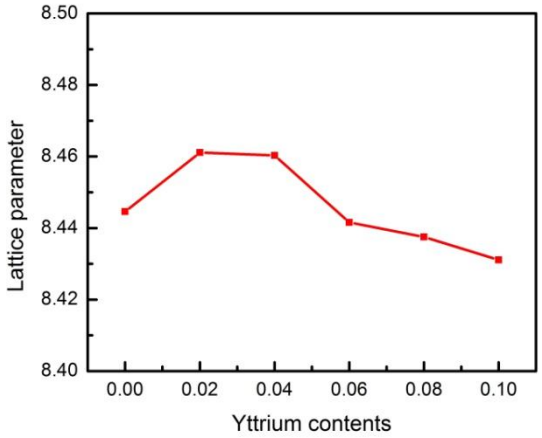

Figure 4.3: Exact lattice parameter 'a_0' of $Mn_{0.5}Zn_{0.5}Y_xFe_{2-x}O_4$ [x = 0.00,0.02, 0.04, 0.06, 0.08 and 0.10] with Yttrium contents

4.1.3 Density and Porosity

The bulk density was measured by usual mass and dimensional consideration whereas X-ray density was calculated from the molecular weight and the volume of the unit cell for each sample by using the equation(3.5) and (3.6).The calculated values of the bulk density and theoretical (or X-ray) density of the present ferrite system are listed in table 4.1. It is observed that bulk density is lower than the X-ray density shown in figure 4.4. This may be due to the existence of pores which were formed and developed during the sample preparation or sintering process.

The bulk density slightly decreases with increasing Y^{3+} ions and the X-ray density increases continuously with increasing Y content. There are two possible existence states of rare earth ions Y^{3+} in the Mn-Zn ferrites: Some of Y^{3+} entered the lattice and substituted the Fe^{3+} ; other Y^{3+} diffused to the grain boundary during the sintering process. Y^{3+} ions entering the lattice can result in the increasing of the lattice

parameter because Y^{3+} ions' larger radius than Fe^{3+} ; But Y^{3+} congregating at grain boundary will reduce lattice parameter due to the vacancies left in the Mn-Zn lattice; As a combination of the two effect described above, a very small overall lattice parameter change can be observed.

Table 4.1: Data of the lattice parameter (a_o), X-ray density (ρ_x), bulk density (ρ_B), porosity (P) of $Mn_{0.5}Zn_{0.5}Y_xFe_{2-x}O_4$ [x = 0.00, 0.02, 0.04, 0.06, 0.08 and 0.10] ferrites sintered at 1200^0C for 2hrs.

X	a_o (Å)	ρ_x (gm/cm^3)	ρ_B (gm/cm^3)	Porosity P (%)
0.00	8.4446	5.6767	4.2786	24.63
0.02	8.4611	5.6711	4.2578	24.93
0.04	8.4603	5.6849	4.2400	25.42
0.06	8.4416	5.7374	4.2057	26.67
0.08	8.4375	5.7604	4.1786	27.46
0.10	8.4311	5.7882	4.1631	28.08

As for the crystallite size reducing, two kinds of Y^{3+} existence states both can constrain the growth of the grain. The Y^{3+} substitution in the lattice will induce lattice distortion, internal stress caused by this distortion hinders the growth of grains. If Y^{3+} diffused to the grain boundaries, that will also restrain the grain growth by lower down the grain mobility. That explains why the crystallite size of the substituted Mn-Zn ferrite is much smaller than un-doped ferrites [4.7- 4.8]. The enhancement of Bulk density is due to activated diffusion process triggered by the excess vacancies created by Fe^{3+} deficiency. Table 4.1 shows the results of lattice parameter, theoretical density, and bulk density shows the results of lattice parameter, theoretical density, and bulk density calculated porosity. It is observed all the samples that porosity increases monotonically with increasing Y^{3+} shown in figure 4.5. Specimens contained some closed porosity. It was difficult to remove these closed porosities completely due to the evaporation of constituents Y replace Fe.

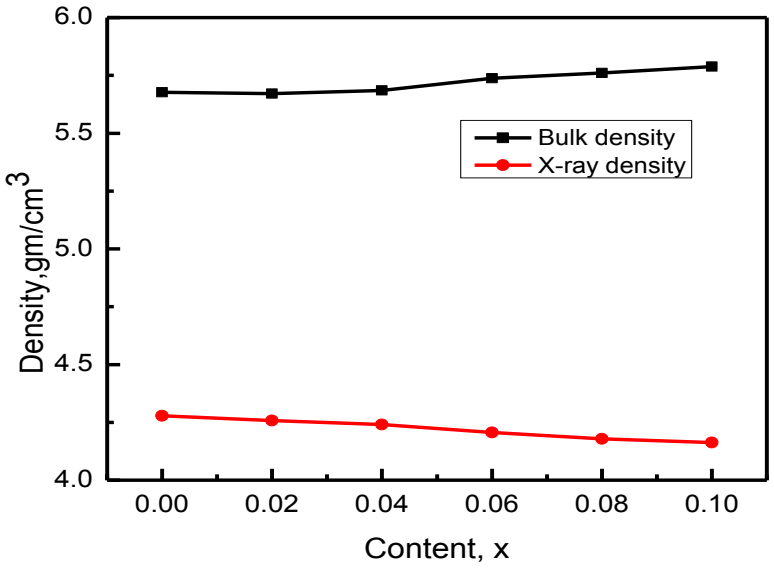

Figure 4.4: Variation of Bulk density and X-ray density as a function of Y content.

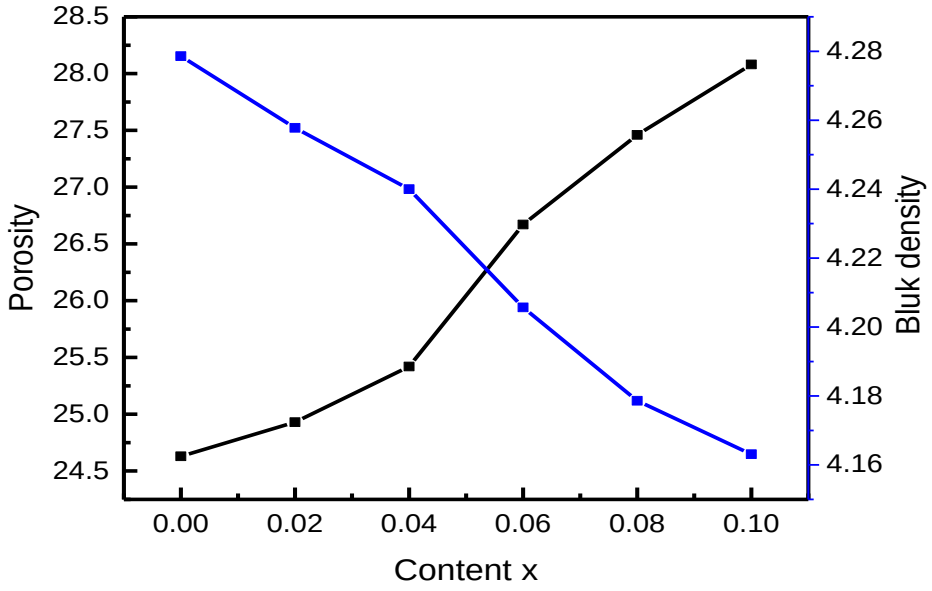

Figure 4.5: Variation of Bulk density and Porosity as a function of Y content

It is known that the porosity of the samples come from two sources, intragranular porosity and intergranular porosity. The intergranular porosity mainly depends on the grain size [4.9]. At higher sintering temperatures the density is decreased because the intergranular porosity is increased resulting from discontinuous grain growth. The porosity which is intrinsic for any oxide material plays an important role in the deciding the magnetic and electrical properties.

4.2 Microstructures

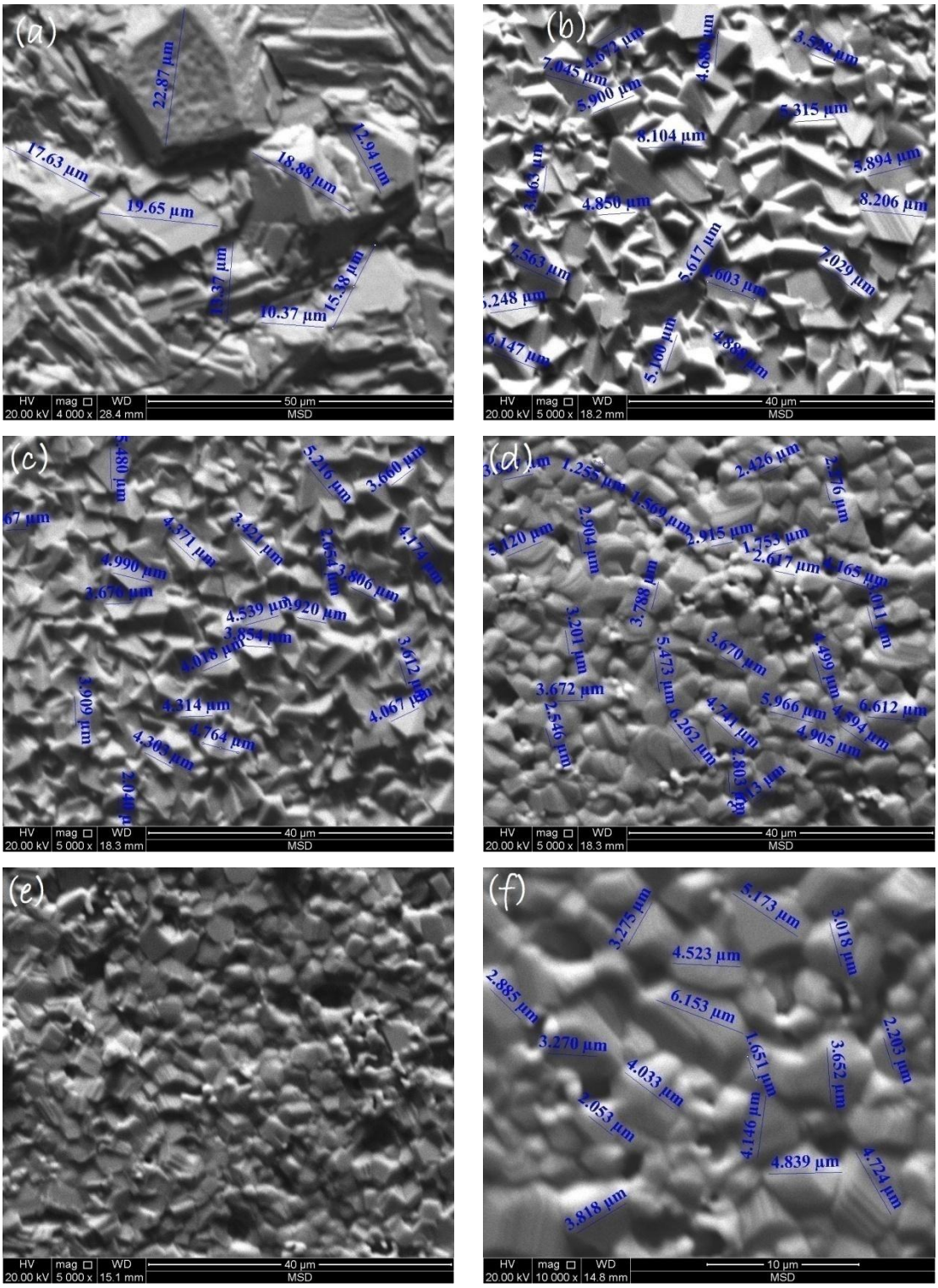

Figure 4.6(a-f): Variation of SEM photographs with Y content (x) of $Mn_{0.5}Zn_{0.5}Y_xFe_{2-x}O_4$ ferrites whose [x = 0.00, 0.02, 0.04, 0.06, 0.08 and 0.10] sintered at 1200^0C for 2 hrs

Microstructure significantly affects the magnetic and electrical properties of ferrites. Grain size is an important parameter affecting the magnetic properties of ferrites. Recrystallization and grain growth involve the movement of grain boundaries. The grain growth, being a result of interparticle mass transport, appears to be dominated by the diffusion mechanism, lattice and grain boundary diffusion [4.10 – 4.11]. The behavior of grain growth reflects the competition between the driving force for grain boundary movement and the retarding force exerted by pores [4.12]. When the driving force of the grain boundary in each grain in homogeneous, the sintered body attains a uniform grain size distribution. Abnormal grain growth occurs if this driving force is inhomogeneous. Moreover, the strength of the driving force depends upon the diffusivity of individual grains, sintering temperatures and porosity.

Figure 4.6(a-f) shows the microstructure of the sample $Mn_{0.5}Zn_{0.5}Y_xFe_{2-x}O_4$ ferrites sintered at 1200^oC for 2hrs. It is clear that the microstructure of Mn-Zn-Y ferrite strongly depend on the amount of Y-content in the samples. The bulk density and grain size decreased with increasing Y content which indicated lower grain growth upon Y-substitution. The net result is that the composition has stoichiometric excess Mn and Zn. It is known that the stoichiometric excess Mn and Zn are used for low temperature liquid phase sintering of the ferrites. For this reason, the densification decreased with Y substitution. As the results Y-content increases replace of Fe content in Mn-Zn-Y ferrites, the grain size decreases gradually shown in table 4.2.

Table 4.2: Grain Size of $Mn_{0.5}Zn_{0.5}Y_xFe_{2-x}O_4$ composites from SEM micrographs with sintering temperature of 1200^0C for 2hrs.

$Mn_{0.5}Zn_{0.5}Y_xFe_{2-x}O_4$	Average grain size (μm)	Initial permeability, μ'
X= 0.00	16	426
X= 0.02	6.0	266
X= 0.04	4.0	202
X= 0.06	3.5	403
X= 0.08	3.0	197
X= 0.10	2.5	175

Figure 4.6(a) sample x = 0, showed the presence of a monophasic single phase homogeneous microstructure with an average grain size 16μm undoped composition whereas Y doped specimens shown in figure 4.6 (b, c, d, e, f) samples x = 0.02, 0.04, 0.06, 0.08 and 0.10 are a biphasic homogeneous microstructure constituted of dark

ferrite matrix grain and small whitish grain at the grain junction/boundary and with grain size decreases monotonically with increases Y content. The Y substituted materials where x = 0.02 to 0.10 show biphasic microstructure consisting of a bigger matrix of ferrite grains and a smaller $YFeO_3$ secondary phase at the grain junctions. The grain size of matrix phase was maximum at x = 0.10 composition for Y content. Relatively lower grain size of ferrite matrix at x =0.10 composition shows in figure 4.6(f) might be due to the grain growth inhibition caused by $YFeO_3$ are clear visible.

4.3 Magnetic Properties

4.3.1 Frequency Dependence of Initial Permeability

The complex permeability is given by $\mu = \mu' - i\mu''$, μ' is the real permeability (in phase) and μ'' the imaginary permeability (90^0 out of phase). Complex permeability has been determined as a function of frequency, f up to 120MHz at room temperature for all the samples of series $Mn_{0.5}Zn_{0.5}Y_xFe_{2-x}O_4$ ferrites by using the conventional technique based on the determination of the complex impedance of circuit loaded with toroid shaped sample. Figure 4.7 represents the results of the real part of the permeability μ' and figure 4.8 imaginary part, μ'' as a function of frequency for the whole series of ferrite samples at 1200^0C for 2hrs.

It is clearly evident from these figures 4.7 that the initial permeability as a function of frequency in the range of 1kHz to 120MHz decreases with Y content, x i.e. the permeability μ' decreases monotonically up to x = 0.10. It is seen that the initial permeability significantly increases at x = 0.06 of Y substitution other doped samples but this lower than x = 0. Decreased in permeability of Mn-Zn ferrites with Y substitution for Fe, where secondary phase $FeYO_3$ is also identified XRD analysis. Y^{3+} has no unpaired electrons and it behaves as diamagnetic. The substitution of ferromagnetic Fe^{3+} ($5\mu_B$) by diamagnetic Y^{3+} for x = 0.06 in the spinel is not useful for increasing permeability. It had been suggested that the substitution of Y^{3+} ion moved $Mn^{2+}$and Zn^{2+} ion from 'B' to 'A' sublattice dilution and increased the magnetic permeability in Mn-Zn ferrites. The decrease in initial permeability at x = 0.02 - 0.10 is probably due to minor precipitation of secondary phase $FeYO_3$. That is, total initial permeability in this case is the sum of the contributions from the spinel and $FeYO_3$ phase. However, the permeability decreased with Y substitution due to presence of higher amount $FeYO_3$ phase.

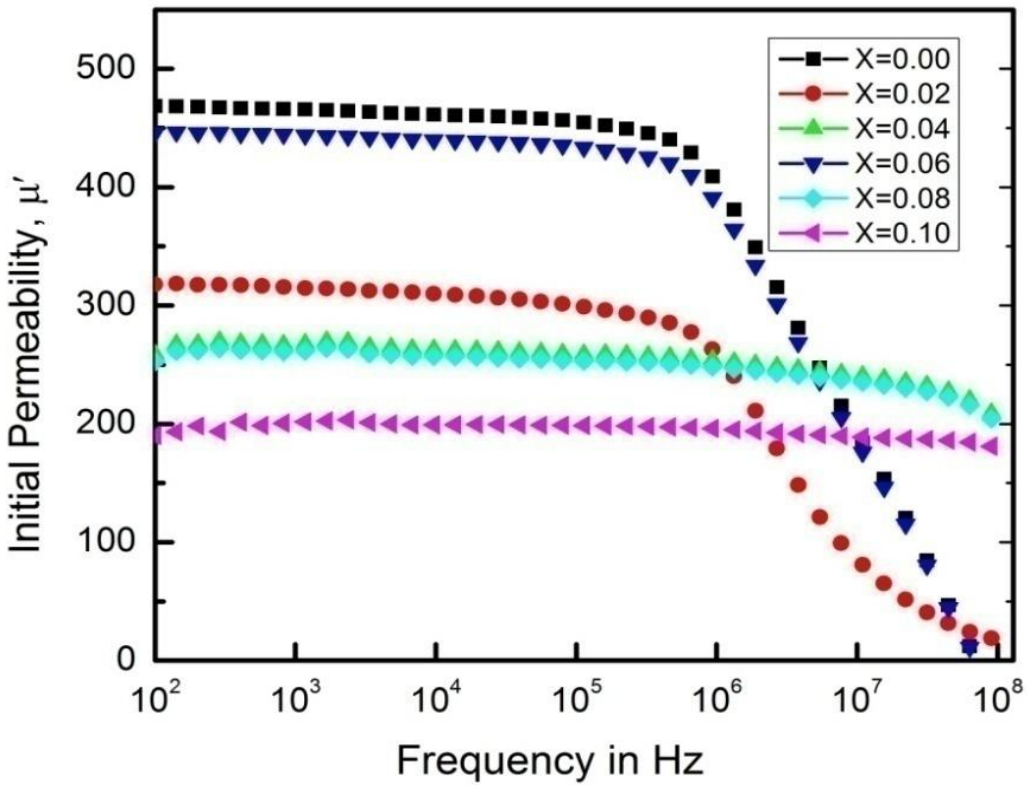

Figure 4.7: Variation of initial permeability with frequency of $Mn_{0.5}Zn_{0.5}Y_xFe_{2-x}O_4$ [x = 0.00, 0.02, 0.04, 0.06, 0.08 and 0.10] ferrites sintered at 1200^0C for 2hrs.

From figure 4.7 it is noticed that the real component of permeability, μ' is fairly constant with frequency up to certain frequency range and then falls rather rapidly to very low value at higher frequency for compositions with x = 0.0, 0.02 & 0.06. The permeability of composition with x = 0.0, 0.02 & 0.06 were stable up to 7 – 9 MHz and then falls rather rapidly to very low value at high frequency. As a result μ' decreases figure 4.7 shows the permeability of the compositions with x = 0.04, 0.08 & 0.10 are stable within the range 80 - 90MHz, the maximum frequency stable limit of the instrumentations.

The constant value of permeability over a wide frequency range, which is named the zone of utility of ferrites, is desirable over various applications such a broad band transformer and wide band read-writes head for video recording [4.13]. The range of operating frequency in the x = 0.04, 0.08 & 0.10 samples are wider than that in the others which shows the compositional stability and quality of the rare earth Y doped ferrites samples.

Table 4.3: Initial Permeability of Mn0.5Zn0.5YxFe2-xO4 composites at different frequency range sintering at the temperature 12000C for 2hrs.

$Mn_{0.5}Zn_{0.5}Y_xFe_{2-x}O_4$	μ' at 100 Hz	μ' at 10 KHz	μ' at 100KHz	μ' at 1 MHz	μ' at 10 MHz	μ' at 100 MHz
X= 0.00	192	199	199	196	189	181
X= 0.02	253	257	253	249	237	212
X= 0.04	260	263	259	255	245	214
X= 0.06	318	310	301	275	88	18
X= 0.08	447	440	436	404	199	------
X= 0.10	469	461	457	422	202	------

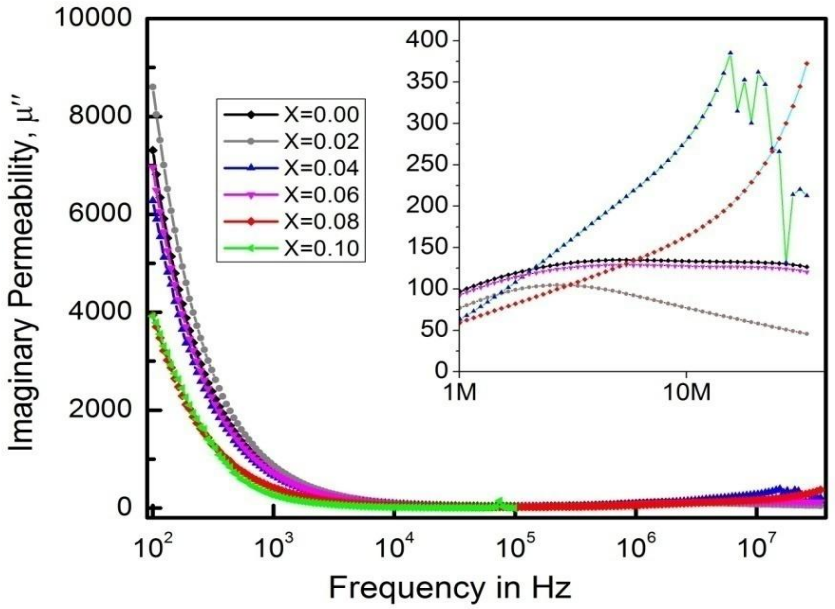

Figure 4.8: Complex imaginary permeability μ" with frequency of $Mn_{0.5}Zn_{0.5}Y_x Fe_2O_4$ [x = 0.00, 0.02, 0.04, 0.06, 0.08 and 0.10] ferrites.

The decrease of permeability with increasing Y may be explained on the basis of intragranular pores entrapped within the grain decreases which create constraint on the domain wall mobility. From the figure 4.8, the imaginary permeability, $\mu^{//}$ initially high at low frequency zone all the samples and then decreases with increasing frequency and almost $\mu^{//}$ constant high frequency range.

The grain growth decreases with increasing Y content diminishes the grain boundary, thereby the domain walls can move easily, which leads to higher permeability. Also during grain growth pores become fewer, which act as independents to domain wall motion due to pinning wall. At high frequencies where at the constant $\mu^{//}$ parameters become more significant, the inductors show high impedance and become resistive and dissipate interfacing signals rather than reflecting these source [4.14]. The operational frequency in the x = 0.04, 0.08 & 0.10

samples is wider than the others sample sintered at 1200^{o}C for 2hrs, because of small grain size and more grain boundaries the permeability is lower that of the others case.

4.3.2 Frequency Dependence of Loss Tangent

Energy loss is an extremely important subject in soft ferrimagnetic materials, since the amount of energy wasted on process other than magnetization can prevent the AC applications of a given material. The ratio of μ″and μ′ is equal tanδ representing the losses in the material are a measure of the inefficiency of the magnetic system. The variation of loss factor, tanδ (= μ″/ μ′) with frequency for all samples has been studied. Figure 4.9 shows the variation of loss factor (tanδ) with frequency for various $Mn_{0.5}Zn_{0.5}Y_xFe_{2-x}O_4$ samples sintered at 1200°C holding time 2 hours. The magnetic losses, which cause the phase shift, can be split up into three components: hysteresis losses, eddy current losses and residual losses. This gives the formula $\tan\delta_m = \tan\delta_h + \tan\delta_e + \tan\delta_r$. As μ'_i is the initial permeability which is measured in presence of low applied magnetic field, therefore, hysteresis losses vanish at very low field strengths.

Thus at low field the remaining magnetic losses are due to eddy current losses and residual losses. Residual losses are independent of frequency. Eddy current losses increase with frequency and are negligible at very low frequency. Eddy current loss can be expressed energy loss per unit volume and is the resistivity [4.15 – 4.16 & 2.8].To Keep the eddy current losses constant as frequency is increased; the resistivity of the material chosen must increase as the square of frequency. Eddy currents are not problem in the Mn-Zn ferrites until higher frequencies are encountered because they have very high resistivity about 10^5Ω-cm to 10^8Ω-cm [4.17]. The ferrite microstructure is assumed to consist of grains of low resistivity separated by grain boundaries of high resistivity. Thicker grain boundaries are preferred to increase the resistance

It is seen from the inset of figure 4.9 that the tanδ decreases with increasing frequency up to 10^8Hz and beyond the frequency 10^8Hz, tanδ increases with the frequency. It is also observed that tanδ value for the Y substituted samples is comparably less than the un-substituted samples at frequency greater than 10^8Hz. It is clear from the figure 4.9 that the value of tanδ is less frequency dependent in the frequency range from 100Hz to 10^8Hz. Therefore, it is concluded that the synthesized

composites have excellent performance in a wide frequency range and can be used for MLCF application, such as embedded inductors or embedded capacitors.

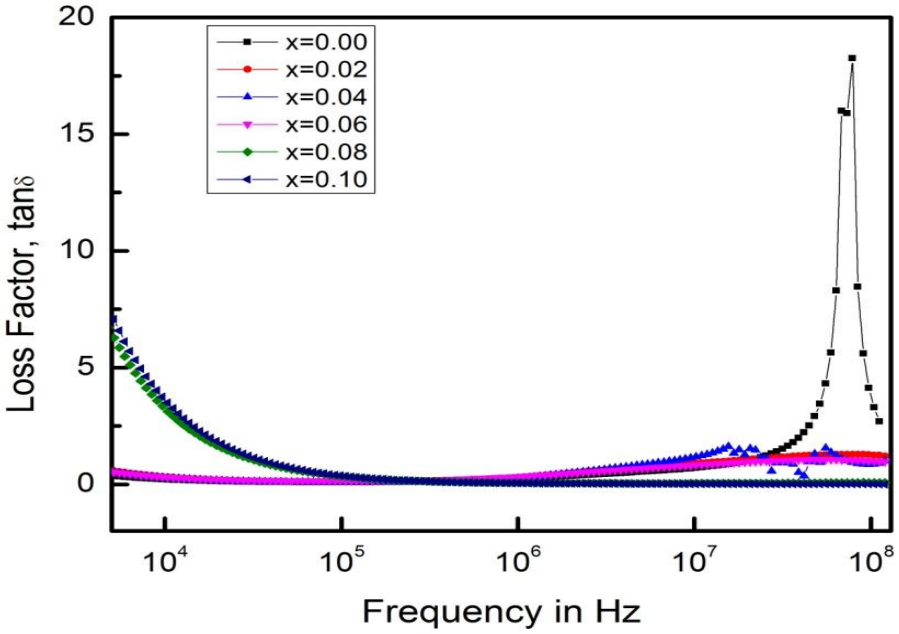

Figure 4.9: Loss Factor tanδ with frequency of $Mn_{0.5}Zn_{0.5}Y_xFe_{2-x}O_4$ [x = 0.00, 0.02, 0.04, 0.06, 0.08 and 0.10] ferrites sintered at 1200^0C for 2hrs.

Table 4.4: Data for Loss Tangent (tanδ) and frequency (f_r) of $Mn_{0.5}Zn_{0.5}Y_xFe_{2-x}O_4$ ferrites sintered at 1200^0C for 2hrs.

$Mn_{0.5}Zn_{0.5}Y_xFe_{2-x}O_4$	Loss tangent (tanδ)	Frequency (Hz)
X= 0.00	0.4	3.7
X= 0.02	0.2	4.2
X= 0.04	0.2	Undefined
X= 0.06	0.1	6.2
X= 0.08	0.3	Undefined
X= 0.10	0.02	Undefined

At lower frequencies, a decrease in magnetic loss is observed. The lag of domain wall motion with respect to the applied magnetic field is responsible for magnetic loss and this is accredited to lattice imperfections [4.18]. At higher frequencies, an increase in loss factor is observed. A resonance loss peak is seen in this increase of magnetic loss. At the resonance, maximum energy transfer occurs from the applied field to the lattice which results the rapid increases in loss factor. As it is observed that phase lag between domain rotation and applied field is greater

than that between applied field and domain wall displacement, the magnetic losses due to domain rotation overrides those due to domain wall displacement [4.19].

4.3.3 Frequency Dependence of Relative quality factor

The frequency dependence of $Mn_{0.5}Zn_{0.5}Y_xFe_{2-x}O_4$ ferrites sintered at 1200^oC for 2hrs have been calculated (RQF = μ''/ tanδ), were calculated by the ratio real part of initial permeability and magnetic loss tangent measured on the coil wound toroidal samples. Figure 4.10 show the frequency dependence RQF showed almost similar trend for all the samples. By increasing Y content, the RQF decreases and the peak associated with the RQF shifting to higher frequencies.

It is observed that the RQF increases with an increase of frequency showing a peak and then decreases with further increase of frequencies and the peak associated with the RQF shifting to lower frequencies. It is seen that RQF deteriorates beyond 10MHz for x = 0, 3MHz for x = 0.02 & 0.04, 5MHz for x = 0.06 and 100MHz for x = 0.08 the loss tangent is minimum. The is due to the loss of domain wall motion with respect to the applied alternating magnetic field and is attributed to various domain defects [4.20], which include non-uniform and non-repetitive domain wall motion, domain wall bowing, localized variation of flux density, nucleation and annihilation of domain walls.

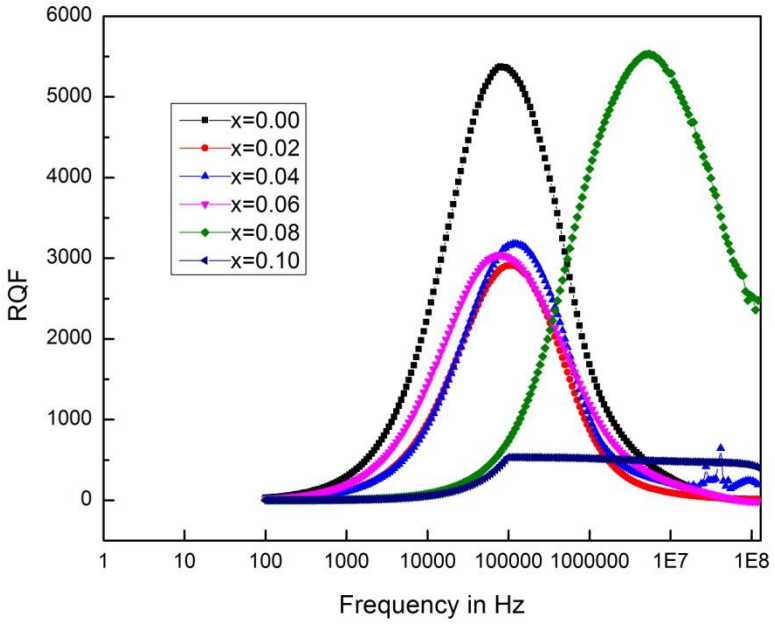

Figure 4.10: Variation of RQF as a function of frequency of $Mn_{0.5}Zn_{0.5}Y_xFe_{2-x}O_4$ ferrites sintered at 1200^0C for 2hrs.

All the samples except x = 0.10 are shown here for better understanding for the merit of the prepared materials for an induction device application. These phenomenon is associated with the ferromagnetic resonance within the range 10kHz to 2MHz for x = 0, 20kHz to 1MHz for x = 0.02 & 0.04, 8kHz to 3MHz and 500kHZ to 100MHz for x = 0.08 at the resonance maximum energy transferred from the applied magnetic field to the lattice resulting in the rapid decrease RQF. Samples with x = 0.08 sintered at 1200^{o}C for 2hrs possess the maximum value of RQF. Mn-Zn-Y ferrites have been found to demonstrate reasonably good permeability at room temperature covering stable wide range of frequency different from different Y content up to several MHz induction and /or core materials.

4.3.4 Variation of Saturation Magnetization at Room Temperature

The room temperature magnetic hysteresis loop of the samples has been measured and is presented in figure 4.11. The hysteresis loops do not show any noticeable hysteresis effect. All samples exhibited low coercivity values inducting that all the samples being to the family of soft ferrites. Figure 4.12 shows the variation of magnetization of the $Mn_{0.5}Zn_{0.5}Y_xFe_{2-x}O_4$ ferrites as a function of applied magnetic field for various samples where x = 0.00, 0.02, 0.04, 0.06, 0.08 and 0.10. It is observed from the figure 4.11 that virgin saturation magnetization (M_S) decrease up to x =0.00 to 0.10. According to Neel's two sublattice model of ferrimagnetism [4.21], M_S is given by $M_S = M_B - M_A$ where M_B and M_A are the octahedral and tetrahedral sublattice magnetizations respectively. In these ferrites Y^{3+} ions occupy the A-sites only.

The decrease in M_S can be explained by the cation distribution in which Y^{3+} ions can convert some of Fe^{3+} to Fe^{2+} in B-sites. Since the magnetic moment of Fe^{2+} is less than that of the Fe^{3+}, therefore the net moment is expected to decrease as well as magnetization. By substituting Y^{3+} ions, it prefers B-sites; therefore magnetic moment in B-sites is decreased, leading to the decrease of the saturation magnetization of the ferrites.

The insignificant decrease of M_s may be experimental uncertainty. The observed variation in M_s can be explained on the basis of cation distribution and the exchange interactions between A- and B-sites. It is observed that the magnetization increases sharply at very low field (H < 3KOe) which corresponds to magnetic domain reorientation that thereafter increases slowly up to saturation due to spin

rotation. This magnetization process is connected with soft magnetic behavior of magnetic material. The slow process of magnetization toward the saturation value is connected with the magnetic anisotropy effect. Actual saturation could not be attained even with magnetic field as high as 12KOe.

From these M – H loops at figure 4.11, the remanance induction (M_r) and coercive force (H_C) were determined shown in table 4.5. The M_S and H_C both decreasing with increasing Y content again M_S and H_C are increasing with increasing Y content, which distinguish reversible and irreversible type's relaxation due to Y^{3+} ions. Irreversible type of relaxation is those which are compared ordering an atomic pair which corresponds to irreversible domain wall movements under external field.

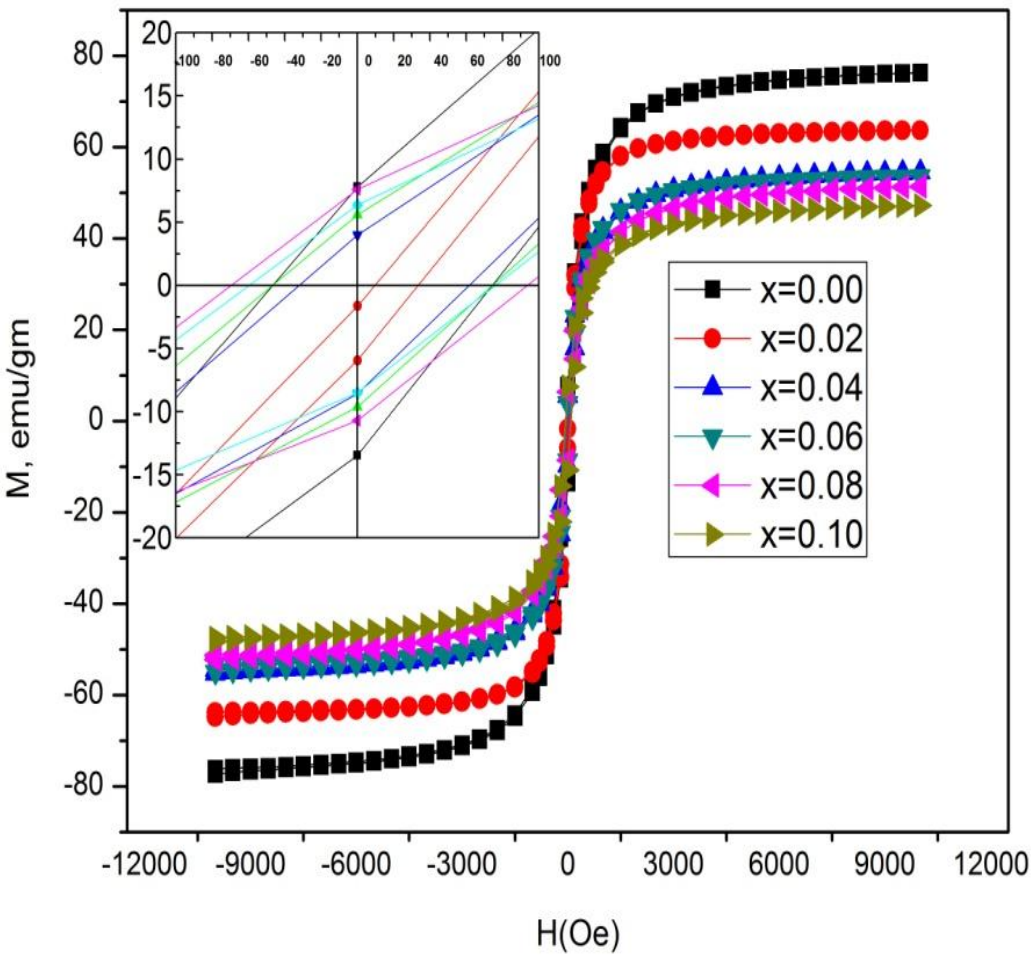

Figure 4.11: Variation of magnetization at room temperature as a function of applied field on $Mn_{0.5}Zn_{0.5}Y_xFe_{2-x}O_4$ ferrites where x = 0.00, 0.02, 0.04, 0.06, 0.08 and 0.10 sintered at 1200^0C for 2hrs.

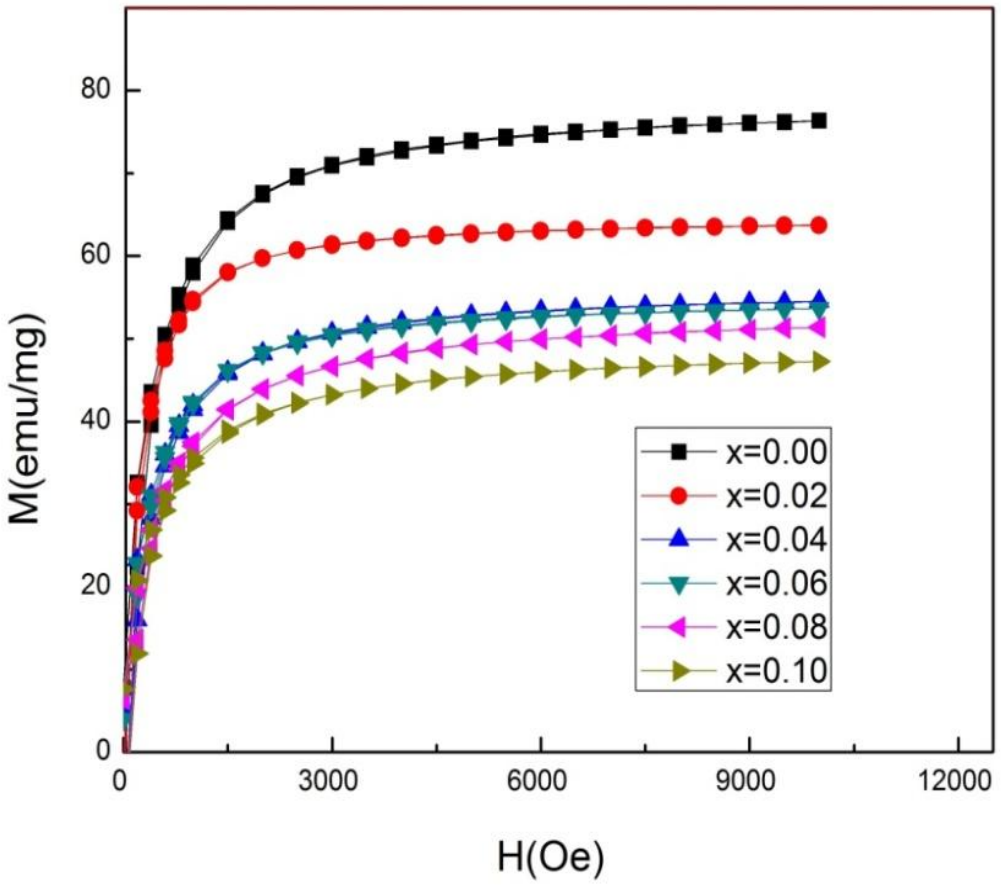

Figure 4.12: Variation of a magnetization at room temperature as a function of applied field on $Mn_{0.5}Zn_{0.5}Y_xFe_{2-x}O_4$ [x = 0.00, 0.02, 0.04, 0.06, 0.08 and 0.10] ferrites sintered at 1200^0C for 2hrs.

Table 4.5: The experimental values of coercive force (H_c), remanence induction (M_r), and saturation Magnetization (M_s),of $Mn_{0.5}Zn_{0.5}Y_xFe_{2-x}O_4$ ferrites at sintering temperature 1200^0C for 2hrs

$Mn_{0.5}Zn_{0.5}Y_xFe_{2-x}O_4$	H_C (Oe)	M_r in emu/g	M_s in emu/g
0.00	61	11	76
0.02	22	04	63
0.04	60	08	54
0.06	46	06	53
0.08	67	07	51
0.10	81	09	47

4.4 Electrical Properties

4.4.1 Temperature Dependence of DC Electrical Resistivity

DC electrical resistivity is an important electrical property of ferrites in high frequency application. The electrical properties of ferrite materials depend upon the method of preparation, chemical composition, grain size and sintering temperature. The temperature dependence of electrical resistivity of $Mn_{0.5}Zn_{0.5}Y_xFe_{2-x}O_4$ ferrites of different compositions has been investigated. Figure 4.13 shows the variation of DC electrical resistivity as a function of temperature of $Mn_{0.5}Zn_{0.5}Y_xFe_{2-x}O_4$ ferrites by using a Keithley Electrometer. It is seen that the electrical DC resistivity decreases with increasing temperature for all studied samples according to equation exhibiting the semiconducting nature of the Y doped Mn-Zn ferrites. Table 4.6 gives the DC electrical resistivity is found to increases with increasing Y content up to x = 0.06 and resistivity found to decrease with further addition of Y content. The resistivity increases with increasing porosity up to x = 0.06, because the charge carriers on their way face less number of pores i.e. obstacles and after $x \geq 0.06$ decrease of resistivity may be attributed to the entrapped intragranular porosity. The resistivity is primarily dependent on the temperature but temperature $\geq 200^oC$ all the samples are independent except x = 0.02 & 0.04.

The relationship between resistivity and temperature has been mentioned in the equation number 2.16.It is seen that the electrical resistivity decreases with $10^3/T$ for all the studied samples according to equation (2.16) exhibiting the semiconducting nature of the samples. From figure one can observe that in the investigated temperature range, the resistivity decreased by about three orders of magnitude. This strong increase in the conductivity with temperature must be regarded mainly as due to the thermally activated mobility of charge carriers, but not to a thermally activated creation of theses carriers.

Table 4.6 shows activation energy for all samples. It is observed that activation energy increasing with increasing Y content. It is noted that the high activation energy goes hand in hand with low conductivity of the ferrite. This is in good accordance with the conclusion that the lower activation energies are associated with higher electrical conductivity while higher activation energies are associated with lower electrical conductivity

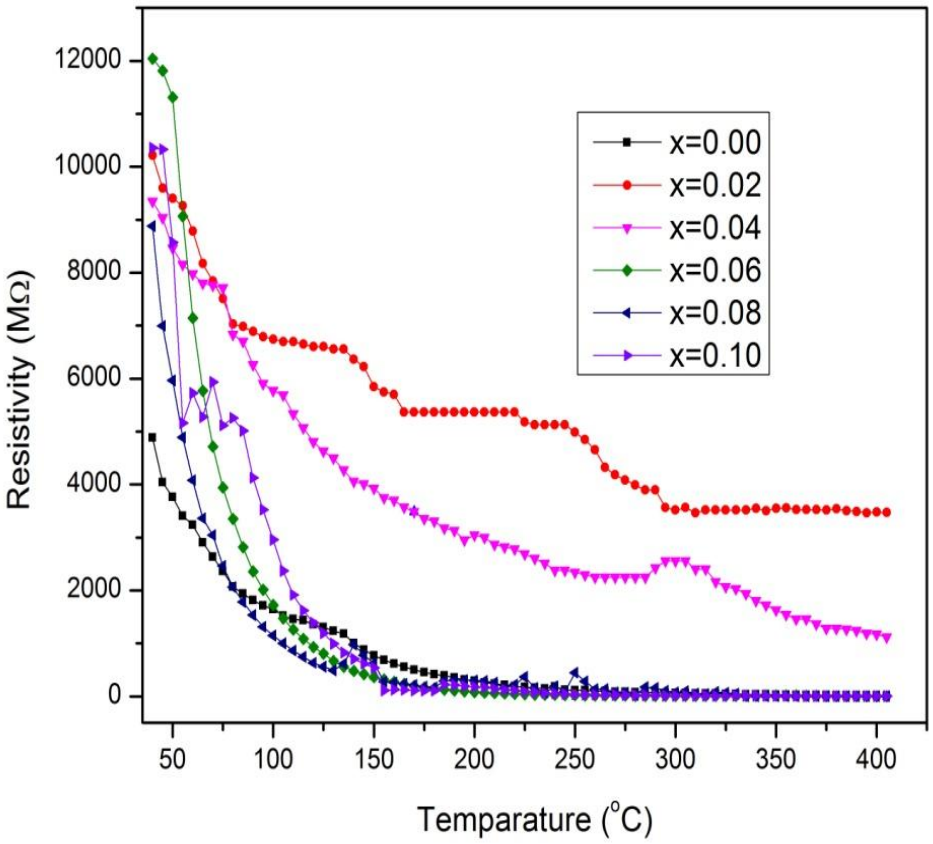

Figure 4.13: Resistivity as a function of Temperature of $Mn_{0.5}Zn_{0.5}Y_xFe_{2-x}O_4$ where x = 0.00, 0.02, 0.04, 0.06, 0.08 and 0.10 ferrites sintered at 1200^0C for 2hrs.

Table 4.6: Activation energy for $Mn_{0.5}Zn_{0.5}Y_xFe_{2-x}O_4$ ferrites at sintering temperature 1200^0C for 2hrs

$Mn_{0.5}Zn_{0.5}Y_xFe_{2-x}O_4$	Activation energy, E_a (eV)	DC electrical resistivity(ρ) at room temperature, Ω-cm
0.00	0.08	5×10^6
0.02	0.085	1.1×10^7
0.04	0.10	9.4×10^6
0.06	0.11	1.2×10^7
0.08	0.095	8.8×10^6
0.10	0.12	1.03×10^7

4.4.2 Frequency Dependence of Dielectric Constant

Figure 4.14 shows the variation of dielectric constant, ε' with frequency for different composition of $Mn_{0.5}Zn_{0.5}Y_xFe_{2-x}O_4$ ferrites sintered at 1200^0C for 2hrs for 1kHz to 120MHz at room temperature. The ε' decreases with increasing frequency,

which is rapid at lower frequencies and slower at higher frequencies. It can be seen from the figure that the dielectric constant is found to decrease continuously with increasing frequency for all the specimens exhibiting a normal dielectric behavior of ferrites. The dielectric dispersion is rapid at lower frequency region and it remains almost independent at high frequency side. The incorporation of Fe into these ferrites has no pronounced effect on the dielectric constant in high frequency, but significantly decreases the dielectric constant in the low frequency range. This is a normal dielectric behavior observed in most of the ferromagnetic materials, which may be due to the interfacial polarization as predicted by Maxwell and Wagner [4.22]. A strong correlation between the dielectric constant and conduction mechanism are available in the literature [4.23].

The dielectric behavior of ferrites may be explained on the basis of the mechanism of the dielectric polarization process and is similar to that of the conduction process. The electronic $Fe^{2+} \leftrightarrow Fe^{3+}$ give the local displacement of electrons in the direction of applied electric field, which induces the polarization in ferrites [4.24]. Dielectric constant of ferrites depends upon the number of available Fe^{2+} ions on the B-sites. The hopping of electrons between Fe^{2+} and Fe^{3+}, and Y^{3+} causes local movements of electrons. Dielectric polarizations arise due to these local displacements of electrons which in turn gives raise the dielectric constant of ferrites.

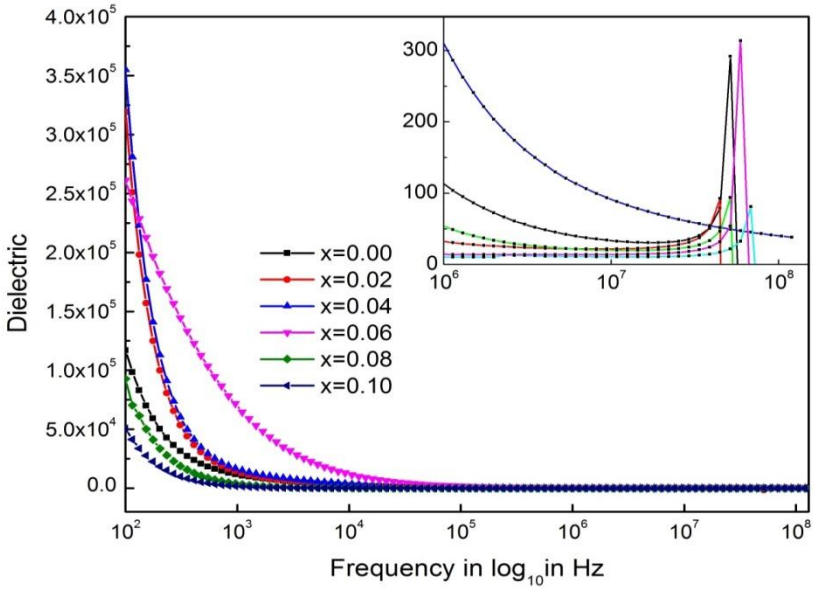

Figure 4.14: Dielectric constant as a function of frequency of the ferrite system of $Mn_{0.5}Zn_{0.5}Y_xFe_{2-x}O_4$ ferrites sintered at 1200^0C for 2hrs.

The magnitude of exchange depends on the concentration Fe^{2+}/Fe^{3+} in pairs present on B-site for the present ferrite. All the samples have high value of $\varepsilon^{/}$ in the order of 10^5 at low frequencies. This could be explained using koop's phenomenological theory [4.25] which was based on the Maxwell-Wagner model [4.22, 4.26] for the inhomogeneous double layer dielectric structure. The first layer is the fairly well conducting large ferrite grain which is separated by the second thin layer of the poorly conducting grain boundaries. The grain boundaries of the lower conductivity were found to be ferrite at lower frequencies while ferrite grains of high conductivity are effective at high frequency.

CONCLUSIONS

5.1 Conclusions

The present research work has been undertaken mainly to investigate the rare earth metal (Y) ions on the structural electrical and magnetic properties of Mn-Zn ferrites. A series of polycrystalline having nominal composition $Mn_{0.5}Zn_{0.5}Y_xFe_{2-x}O_4$ where x = 0.00, 0.02, 0.04, 0.06, 0.08, 0.10 have been prepared by the standard solid state reaction method sintered at 1200ºC for two hours. The effects of Y^{3+} on substitution on Mn-Zn ferrites have imparted significant change in structural, microstructural, magnetic and electrical resistivity properties.

From this Study the following conclusions can be outlined:

(i) The Y substitution for Fe in the $Mn_{0.5}Zn_{0.5}Y_xFe_{2-x}O_4$ ferrites mainly produced secondary phase $YFeO_3$. The lattice parameter increases initially due the replacement of Fe^{3+} ions by the larger Y^{3+} ions in the octahedral sites after increasing Y content no significant decrease in lattice parameter is observed in the present experiment.

(ii) The bulk density is lower than the X-ray density due to the existence of pores which are formed developed samples are preparation or sintering process. The bulk density slightly decreases with increasing Y content and X-ray density increases continuously with increasing Y content. Porosity increases monotonically with increasing Y content but contained some closed porosity due to the evaporation of constituents Y replace Fe.

(iii) SEM micrographs indicate the grain size decreased with increasing Y content which indicated lower grain growth. In the absence of Y content in Mn-Zn ferrite of a monophasic single phase homogeneous microstructure with an average grain size ~16μm but Y doped specimen are a biphasic homogeneous microstructure of dark ferrite matrix grain and small whitish grain at the grain boundary and with grain size decreases monotonically with increases Y content.

(iv) The initial permeability decreases with increasing Y content due to secondary phase of $YFeO_3$ segregated in the prepared samples. The maximum permeability undoped Mn-Zn ferrite value of μ_i = 426 and Y doped for the sample x = 0.6 value of μ_i = 403 after decreasing. The permeability of the compositions with x = 0.04 & 0.08 are stable up to the

range 80 - 90MHZ, the maximum frequency stable limit of the instrumentations. The highest RQF found for the sample x = 0.08 is 5500 & x = 0.04 is 3000. All the samples $Mn_{0.5}Zn_{0.5}Y_xFe_{2-x}O_4$ except x = 0.10 are shown for better understanding for good permeability at room temperature covering stable wide range of frequency different from different Y content up to several MHz range.

(v) Magnetization increases sharply at very low field (H < 3kOe) which corresponds to magnetic domain reorientation due to domain wall displacement and there after increase slowly up to saturation due to spin rotation for Y doped in Mn-Zn ferrites. Saturation magnetization decreases with increasing both Y substituted Fe in Mn-Zn ferrites can be explained on the basis of cation distribution and exchange interaction A- and B-sites.

(vi) The DC electrical resistivity is found to decrease with increasing temperature for all studied samples which means Y doped Mn-Zn ferrites are semiconducting nature.

(vii) Dielectric constant decreases with increasing frequency exhibiting normally dielectric behavior of ferrites like all the samples. The dielectric dispersion is rapid at lower frequency region and remains almost independent at high frequency region. The increases in frequency enhance the hopping frequency of charge carriers, resulting in an increase in the conduction process, thereby decreasing the dielectric constant.

5.2 Scope for Future Work

Some studies on different aspects are possible for fundamental interest and also for potential applications of the studied rare earth doped ferrite materials. These modern devices exclusively need soft ferrite materials are used in inductors which form a basic requirement in high technology areas. Mn-Zn-Y ferrites are suitable for these devices for future.

The scopes of the future works are proposed as:

(i) Different spinel ferrite systems to investigate the effect on lowering the sintering temperature are improving electromagnetic properties.

(ii) Neutron diffraction analysis may be performed for these compositions to determine the distribution of substituted Y^{3+} ions between A- and B-sites. Mossbauer spectroscopy can also be studied.

(iii) Fabrication and characterization of multilayer chip inductor using improved Mn-Zn-Y ferrites as stated.

(iv) Some AC and DC electrical properties may be studied.

(v) For the domain wall motion and degree of ordering present in the samples, MFM study can carried out.

REFERENCES

CHPATER-I

[1.1] Akashi T.; "Effect of Rare Earth Substitution on Magnetic and Electrical Properties of Mn–Zn Ferrites". Inst. Tran. Jpn Met. 2, 171, 1961.

[1.2] Hossain M. A., Khan M. N. I. and Sikder S. S.; "Structural Magnetic and Dielectric Behaviors of Y^{3+} Substituted Ni-Zn Ferrites", International Journal of Nano Science Trends and Technology, 1, 2, 1-19, 2017.

[1.3] Modak S., Ammar M., Mazaleyrat F., Das S., and Chakrabarti P. K.; "XRD, HRTEM and Magnetic Properties of Mixed Spinel Nanocrystalline Ni–Zn–Cu-Ferrite", J. Alloys Compd. 473, 15, 2009.

[1.4] Dahotre S. G. and Singh L. N.; "Study of Magnetic Properties of Nanostructure Mn-Zn Ferrite", Archives of Physics Research, 2 (1): 81-89, 2011.

[1.5] Su H., Zhang H. W., Tang X. L., and Shi Y.; "Improving Soft Magnetic Properties of Mn-Zn Ferrite by Rare Earth ions Doping", J. Alloys Compd. 468, 290, 2009

[1.6] Rezlescu N., Rezlescu E., Pasnicu C., Craus M. L.; "Effect of the Rare Earth Metal of Some Properties of Nickel-Zinc Ferrite", J. Phys. Condens. Matter, 6, 5707, 1994.

[1.7] Satter A. A. and El-Shokrofy K. M.; J. "Rare Earth Doping Effect on the Electrical Properties of Cu-Zn Ferrites" ,Physics.IV CI, 245, 1997.

[1.8] Shokrollahi H.; "Magnetic Properties and Densification of Manganese–Zinc Soft Ferrites ($Mn_{1-x}Zn_xFe_2O_4$) Doped With Low Melting Point Oxides", J. Magn. Magn. Mater. 320, 463, 2008.

[1.9] Shaikh P. A., Kambale R. C., Rao A. V., Kolekar Y. D.; "Studies on Structural and Electrical Properties of $Co_{1-x}Ni_xFe_{1.9}Mn_{0.1}O_4$ Ferrite", J. Alloys Compd. 482, 276, 2009 .

[1.10] Calderón-Ortiz E., Perales-Perez O., Voyles P., Gutierrez G. and Tomar M. S.; "$Mn_xZn_{1-x}Fe_{2-y}R_yO_4$ (R=Gd, Eu) Ferrite Nanocrystals for Magnetocaloric Applications" Microelec. J. 40, 677, 2009.

[1.11] Hossain M. A., Khan M. N. I. and Sikder S. S.; "Effect of Resistivity, Permeability and Curie Temperature of Rare Earth Metal Europium (Eu)

Substitution on $Ni_{0.60}Zn_{0.40-x}Eu_xFe_2O_4$(x = 0.05, 0.10, 0.15) Ferrites", ARPN Journal of Science and Technology, Vol. 5, No. 10, pp. 520-524, 2015.

[1.12] Hilpert, S.; Ber. Deutsh. " Magnetic Properties of Ferrite and Iron Oxide", Chem. Ges. BD2, Vol.42, pp. 2248-2261, 1909.

[1.13] Snoek, J. L., "Magnetic and Electrical Properties of the Binary Systems $MO.Fe_2O_3$", physica, Vol.3, pp.463-483, 1936.

[1.14] Smit J.; "Magnetic Properties of Materials", Macgraw Hill, New York, 1997.

[1.15] Takai T.; "Introduction to Magnetic Ferrites and Nanocomposites", J. Electr. Chems. Japan, Vol. 5, pp.411, 1937.

[1.16] Uma Shankar Sharma, Ram Naresh Sharma and Rashmi Shah " Physical and Magnetic Properties of Manganese Ferrite Nanoparticles" August 2014.

[1.17] Isfahani M. J. N., Myndyk M., Menzel D., Feldhoff A., Amighian J. and Sepelak V.; "Magnetic Properties of Nanostructured Mn-Zn Ferrites", J. Magn. Magn. Mater., 321, 152 – 156, 2009.

[1.18] Ping Hu, Yang H., Pan D., Wang H., Tian J., Zhang S., Wang X. and Volnsky A. A.; "Heat Treatment Effects on Microstructure and Magnetic Properties of Mn-Zn Ferrite Powders", J. Magn. Magn. Matter., 322, 173 – 177, 2010.

[1.19] Ahmed M. A., Okasha N. and Sayed M. M. E; **"**Enhancement of the Physical Properties of Rare-Earth Substituted Mn–Zn Ferrites Prepared by Flash Method" Cera Intern. 33(1), 49, 2007.

[1.20] Zhao L., Cui Y., Yang H., Yu L., Jin W. and Feng S.; ''Study on Magnetic Properties of Nanocrystalline La-, Nd-, or Gd-Substituted Ni–Mn Ferrite at Low Temperatures'' Mat. Lett., 60, 104, 2006.

[1.21] Rezlescu N., Rezlescu E., Popa P. D. and Rezlescu L.; "Effects of Rare-Earth Oxides on Physical Properties of Li–Zn Ferrite", J. Alloy Compd., 275 – 277, 657, 1998.

[1.22] Sun J., Li J. and Sun G.; "A Novel Architecture of the 3D Stacked MRAM L2 Cache for CMPs", J. Magn. Magn. Matter., 25, 20, 2002.

[1.23] Nakamura T., "Low Temperature Sintering of Ni – Cu- Zn Ferrite and Its Permeability Spectra", J. Magn. Magn. Mater., 168, 285 – 291, 1997.

[1.24] Zhong X. C., Guo X. J., Zou S. Y., Yu H. Y., Liu Z. W., Zhang Y. F. and Wang K. X.; "Soft Magnetic Properties of Mn-Zn Ferrite by Rrare Earth ions Doping", AIP ADVANCES 8, 047807, 2018.

CHPATER-II

[2.1] Rare Earth Elements - Critical Resources for High Technology: United States Geological Survey; Fact Sheet 087-02.

[2.2] Jing J., Liang-Chao L., Feng X.; "Preparation, Characterization and Magnetic Properties of PANI/La-substituted LiNi Ferrite Nan Composites", Chin. J. Chem. 24, 1804, 2006.

[2.3] Jing J., Liang-Chao L., Feng X.; "Structural Analysis and Magnetic Properties of Gd-Doped Li-Ni Ferrites Prepared Using Rheological Phase Reaction Method**",** J. Rare Earths.25, 79, 2007.

[2.4] Vanuitert L. G.; "High-Resistivity Nickel Ferrites—the Effect of Minor Additions of Manganese or Cobalt". J. Chemi. Phys. 23, 1883, 1955.

[2.5] Kolekar C. B., Kamble P.N., Vaingankar A.S.; "Thermoelectric Power in Gd^{3+}-substituted Cu-Cd Ferrites", J. Bull. Mater. Sci. 18(2), 133, 1995.

[2.6] Jie S., Lixi W., Naicen X., Qitu Z.; "Introduction to Ferrite", J. Rare Earths, 28, 445, 2010.

[2.7] Bahadur D. Giri J. Nayak B. B, Sriharsha T., Pradhan P., Prasad N. K.; "Processing, Properties and Some Novel Applications of Magnetic Nanoparticles" 2J. Pramana Phys., 65, 663, 2005.

[2.8] Valenzuela R.; "Magnetic Ceramics", Cambridge University Press, Cambridge 1994.

[2.9] Murdock E. S., Simmons R. F., Davidson R.; Roadmap for 10 Gbit/in2 Media: Challenges. IEEE Trans. Magnetics, 28, 5, 3078, 1992.

[2.10] Wulfsberg G.; "Inorganic Chemistry", University Science Books, 691, 2000.

[2.11] Standly K. J, "Oxide Magnetic Materials", 2nd ed., Oxford University Press, 1972

[2.12] Vijaya M. S. and Rangarajan G.; "Materials Science", McGraw-Hill Publ. Comp. Ltd., New Delhi, 447, 1999-2002.

[2.13] Van Uitert L. G.; "High-Resistivity Nickel Ferrites – The Effect of Minor Additions of Manganese or Cobalt", J. Chem. Phys. 24(2), 306-310, 1956.

[2.14] Virginia Fuentes, Aburto S. and Velenzuela R.; "Sub lattice in Nickel Ferrite." J. Magn. Magn. Mater., 69, 233, 1987.

[2.15] Anderson P. W.; "π-Electron Magnetism: From Molecules to Magnetic Materials", Vol 1, Eds, G. T. Rado and H. Shul; Academic Press, New York, 1963.

[2.16] Samokhvalov A. A. and Rustamov A. G.; SOV. Phys. Solid State, 6, 749, 1964.

[2.17] Verway E. J. W., Heilmann E. L. and Romeijin F. C.; "Physical Properties and Cation Arrangement of Oxides with Spinel Structure 11. Electronic Conductivity", J. Chem. Phys. 15(4), 181-187, 1947.

[2.18] Jonker G. H.; "Analysis of the Semiconducting Properties of Cobalt Ferrite", J. Phys. Chem. Solids, 9(2), 165-175, 1959.

[2.19] Smit and Wijn W. J. P.; "Ferrites", Philips Technical Libery C Wiley, New York, 1959.

[2.20] Goldman A.; "Handbook of Modern Ferromagnetic Materials", Kulwer Acad. Pub, Boston, U.S.A 1999.

[2.21] M. F. Yan and D. W. Johnson, "Impurity Induced Exaggerated Grain Growth in Mn-Zn Ferrites," *J.* Am. Ceram. Soc., 61, 342, 1978.

Chapter III

[3.1] Kittel C.; "Introduction to Solid State Physics", 7th edition, John Wiley & Sons, Inc., Singapore, 1996.

[3.2] Nelson J. B., Riley D. P; "An Experimental Investigation of Extrapolation Methods in the Derivation of Accurate Unit-Cell Dimensions of Crystals", Proc. Phys. Soc. London 57, 160, 1945.

[3.3] Kin O. Low, Frank Sale R.; "Electromagnetic Properties of Gel-Derived Ni-Cu-Zn Ferrites." J. Magn. Magn. Mater., 246, 30 - 35, 2002.

[3.4] Tahir Abbas, Islam M. U. and Ashraf Ch M.; "Study of Sintering Behavior and Electrical Properties of Cu-Zn-Fe-O System", Mod. Phy. Letts., B 9(22), 1419, 1995.

[3.5] Simon Forner; "Versatile and Sensitive Vibrating Sample Magnetometer", Rev. Sci. Instr. 30, P.548, 1959

[3.6] Hossain A. K. M. A.; "Investigation of Colossal Magnetoresistance in Bulk and Thick Film Magnetites*",* Ph. D. Thesis, Imperial College, London, 1998.

Chapter IV

[4.1] Ovidiu F. Caltun, Leonard Spinu; "Magnetic Properties of High Frequency Ni-Zn Ferrites Doped with CuO", Trans. Magn., Vol.37, No.4, July 2001.

[4.2] Goldman A.; "Hand book of Modern Ferromagnetic Metals", Kulwer Academic Publishers, Boston, USA, 1999.

[4.3] Akhter Hossain A. K. M., Mahmud S. T., Seki M., Kawai T. and Tabata H.; "Structural, Electrical Transport and Magnetic properties of $Ni_{1-x}Zn_xFe_2O_4$", J. Magn. Magn. Mater., 312, 210, 2007.

[4.4] Zhao L., Cui Y., Yang H., Yu L., Jin W. and Feng S.; "The Magnetic Properties of $Ni_{0.7}Mn_{0.3}Gd_xFe_{2-x}O_4$ Ferrite", Mater. Lett., 60, 104, 2006.

[4.5] Ashok Gadkari, Tukaram Shinde and Pramod Vasambekar; "Influence of Rare Earth ions on Structural and Magnetic Properties of $CdFe_2O_4$ Ferrites", RARE METALS, Vo.29, No. 2, p.168, Apr. 2010.

[4.6] Nelson J. B., Riley D. P.; "An Experimental Investigation of Extrapolation Methods in the Derivation of Accurate Unit-Cell Dimensions of Crystals"; Proc. Phys. Soc. London 57, 160, 1945.

[4.7] Sun G., Li J., Sun J. and Yang X.; "The Influences of Zn2+ and Some Rare Earth Ions on the Magnetic Proper-ties of Nickel-Zinc Ferrites", J. Magn. Magn. Mater., 281, 173 - 177, 2004.

[4.8] Jacobo S. E., Fano W. G. and Razzitte A. C.; "The Effect of Rare Earth Substitution on the Magnetic Properties of $Ni_{0.5}Zn_{0.5}M_xFe_{2-x}O_4$ (M: Rare Earth)", Physica B., 320, 261 - 263, 2002.

[4.9] Yang Z. H., Gong Z., Q., Li H. X., Ma Y. T. and Yang Y. F., " Synthesis of Ni-Zn Ferrites and Its Microstructure and Magnetic Properties", Journal of Central South University of Technology, 13, 618 - 623, 2006.

[4.10] Gupta T. K. and Coble R. L.; "Sintering of ZnO: I, Densification and Grain Growth", J. Am. Ceram. Soc., 51, 521, 1968.

[4.11] Coble R. L. and Gupta T. K.; "Sintering and Related Phenomena", G. C. Khcznski, N. A. Hroton and C. F. Gibbon (eds.) p.423, Gordon and Breach, New York, 1967.

[4.12] Bellad S. S., Watawe S. C. and Chougule B. K.; "Microstructure and Permeability Studies of Mixed Li-Cd Ferrites", J. Magn. Magn. Mater., 195, 57, 1999.

[4.13] Verma A. and Chatterjee R.; "Effect of Zinc Concentration on the Structural, Electrical and Magnetic Properties of Mixed Mn-Zn and Ni-Zn Ferrites Synthesized by the Citrate Precursor Technique"; J. Magn. Magn. Mater. 306, 313 – 320, 2006.

[4.14] Snelling E. C.; "Soft Ferrites; Properties and Applications", Ed. Butterworth, London, 1988.

[4.15] Shrotri J. J., Kulkarni S. D., Deshpande C. E. and Date S. K.; "Effect of Cu Substitution on the Magnetic and Electrical Properties of Ni-Zn Ferrite Synthesized by Soft Chemical Method", Mater. Chem. Phys. 59, 1, 1999.

[4.16] Tsutaoka T., Ueshima, Tokunaga M., Nakamura T. and Hatakeyama K.; "Frequency Dispersion and Temperature Variation of Complex Permeability of Ni-Zn Ferrite Composite Materials", J. Appl. Phys., 78(6), 3983, 1995.

[4.17] Brailsford F.; "Physical Principles of Magnetism", D. Van Nostrand company Ltd., London, 1996.

[4.18] Cullity B. D.; "Introduction to Magnetic Materials", Addision - Wisley Publishing Company, Inc., California, 1972.

[4.19] Rado G.T., Wright R.W., Emerson W. H. and Terris A.; "Ferromagnetic at Very High Frequencies. IV. Temperature Dependence of the Magnetic Spectrum of a Ferrite", Physical Review, Vol-88, pp 909-915, 1952

[4.20] Chauhan B. S., Kumar R., Jadhav K. M. and Singh M.; "Magnetic Study of Substituted Mg-Mn Ferrites Synthesized by Citrate Precursor Method", Journal of Magnetism and Magnetic Materials, Vol. 283, pp 71 - 81, 2004.

[4.21] Neel I.; "Propriétés Magnétiques Des Ferrites ; Ferrimagnétisme et Antiferromagnétisme", Ann. Phys. 3, 137, 1948.

[4.22] Maxwell J.; 1873, "Electricity and Magnetism", Vol.1, Oxford University Press. London Wanger K., Ann. Phys. 40, 817, 1913.

[4.23] Nutan Gupta, Kashyap S. C. and Dube D. C.; "Dielectric and Magnetic Properties of Citrate Route Processed Li-Co Spinel Ferrites", Phys. Stat. Solidi (a), 204(7), 2007.

[4.24] Zhenxing Yue, Zhou Ji, Longtu Li, Xiaolui Wang and Zhilun Gui; "Effect of Copper on the Electromagnetic Properties of Mg-Zn-Cu Ferrites Prepared by Sol-gel Auto-Combustion Method", Mater. Sci. Eng. B, 86, 64, 2001.

[4.25] Koops C. G.; "On the Dispersion of Resistivity and Dielectric Constant of Some Semiconductors at Audio Frequencies", Phys. Rev., 83, 121, 1951.

[4.26] Venugopal Reddy P. and Seshagiri Rao T.; "Dielectric Behavior of Mixed Li-Ni Ferrites at Low Frequencies", J. Less Common Met., 86, 255, 1982.

CONFERENCE PUBLICATIONS

1. **S. S. Acharjee**, M. A. Hossain, M. N. I. Khan and S. S. Sikder; "Study of the Structural and Magnetic Properties of Rare Earth Yttrium Doped Mn-Zn Ferrites", International Conference on Physics 2018, 08-10 March, DU, Dhaka-1000, Bangladesh
2. M. A. Hossain, **S. S. Acharjee**, M. N. I. Khan and S. S. Sikder;; "Complex Permeability of Yttrium (Y) Substituted Mn-Zn Rare Earth Ferrites Prepared by Solid State Reaction Technique"; Conference on Whether Forecasting and Advances in Physics, 11-12 May, 2018, KUET, Khulna-9203, Bangladesh
3. **S. S. Acharjee**, M. A. Hossain, M. N. I. Khan and S. S. Sikder; "Structure and Transport Properties of Yttrium (Y) Substituted Mn-Zn Rare Earth Ferrites Prepared By Soild State Reaction Method", Conference on Whether Forecasting and Advances in Physics, 11-12 May, 2018, KUET, Khulna-9203, Bangladesh